NASA TECHNICAL MEMORANDUM

NASA TM X-2294

NASA TM X-2294

MACH 2.5 PERFORMANCE OF A BICONE INLET WITH INTERNAL FOCUSED COMPRESSION AND 40-PERCENT INTERNAL CONTRACTION

by Joseph F. Wasserbauer and David A. Choby

Lewis Research Center
Cleveland, Ohio 44135

NATIONAL AERONAUTICS AND SPACE ADMINISTRATION • WASHINGTON, D. C. • MAY 1971

1. Report No.	2. Government Accession No.	3. Recipient's Catalog No.
NASA TM X-2294		

4. Title and Subtitle	5. Report Date
MACH 2.5 PERFORMANCE OF A BICONE INLET WITH INTERNAL FOCUSED COMPRESSION AND 40-PERCENT INTERNAL CONTRACTION	May 1971
	6. Performing Organization Code
7. Author(s)	8. Performing Organization Report No.
Joseph F. Wasserbauer and David A. Choby	E-6079
	10. Work Unit No.
9. Performing Organization Name and Address	720-03
Lewis Research Center National Aeronautics and Space Administration Cleveland, Ohio 44135	11. Contract or Grant No.
	13. Type of Report and Period Covered
12. Sponsoring Agency Name and Address	Technical Memorandum
National Aeronautics and Space Administration Washington, D.C. 20546	14. Sponsoring Agency Code

15. Supplementary Notes

16. Abstract

The inlet was designed to have the minimum internal contraction consistent with high total-pressure recovery and low cowl drag. Without a bypass system the inlet provided a critical pressure recovery of 0.880 and a steady-state distortion of 0.185 when the supercritical bleed flow was 0.032. With a bypass system in operation the critical pressure recovery increased to 0.903 and the steady-state distortion dropped to 0.10. Maximum angle of attack before an inlet unstart ranged as high as 9.4^{o}.

17. Key Words (Suggested by Author(s))	18. Distribution Statement
Supersonic cruise inlets Inlets Propulsion systems	Unclassified - unlimited

19. Security Classif. (of this report)	20. Security Classif. (of this page)	21. No. of Pages	22. Price*
Unclassified	Unclassified	58	$3.00

*For sale by the National Technical Information Service, Springfield, Virginia 22151

MACH 2.5 PERFORMANCE OF A BICONE INLET WITH INTERNAL FOCUSED COMPRESSION AND 40-PERCENT INTERNAL CONTRACTION

by Joseph F. Wasserbauer and David A. Choby

Lewis Research Center

SUMMARY

An investigation was conducted to determine the performance characteristics of an axisymmetric, bicone, mixed-compression inlet system designed for Mach 2.5 operation. Forty percent of the supersonic area contraction occurred internally, which is the minimum amount consistent with high total-pressure recovery and low cowl drag. The internal compression from the cowl surface was focused on the centerbody shoulder. Porous bleed regions were located on the cowl and a bleed slot was located on the centerbody shoulder. The study was conducted at Mach 2.5 and at a Reynolds number of 2.5×10^6 per foot (8.2×10^6/m).

Without a bypass system the inlet provided a critical pressure recovery of 0.880 and a steady-state distortion of 0.185 when the supercritical bleed flow was 0.032. Addition of vortex generators to the centerbody decreased distortion to 0.135. For supercritical operation, maximum angle of attack before an inlet unstart was 8.5°. For critical operation it decreased to 4.8°.

With a bypass system in operation the critical pressure recovery increased to 0.903 and the steady-state distortion dropped to 0.10.

The dynamic distortion level was 0.02 at critical operation. A reduction of cowl bleed was made to decrease the supercritical bleed flow to 0.025. With the addition of vortex generators on the cowl and centerbody a critical pressure recovery of 0.885 was attained with a steady-state distortion level of only 0.045.

INTRODUCTION

Supersonic inlets should be able to operate efficiently with low drag over the entire flight range of the airplane. For flight speeds above Mach 2.0, mixed-compression inlets offer this capability. Typical mixed-compression inlets designed for operation

above Mach 2.0 are described in references 1 to 4. The inlets of references 1 to 3 are axisymmetric, single-cone inlets which require either collapsing or translating centerbodies to vary the contraction ratio. The inlet of reference 4 is two dimensional and its contraction ratio is varied by movable ramp surfaces.

The design philosophy for the axisymmetric, mixed-compression inlet of this investigation was to use a two-cone spike to provide the maximum external compression compatible with high total-pressure recovery and low cowl drag. To vary contraction ratio the second cone would be collapsed, and at its lowest position it would blend into the first-cone contours so as to provide a single-cone centerbody. This approach avoids the sharp curves that normally result when a single-cone surface is collapsed. This philosophy provided 40 percent of the supersonic area contraction internally for a design Mach number of 2.5. This inlet was designed such that the isentropic compression fan from the cowl and the cowl-lip oblique shock were focused on the centerbody at one point. This compression was cancelled at the centerbody with an abrupt turn, in the manner described in reference 5. The present investigation evaluates inlet performance using several bleed locations and bleed flow rates. Flow surveys were made just downstream of the throat region, midway in the subsonic diffuser, and at the diffuser exit to evaluate local flow conditions.

The test was conducted in the Lewis 10- by 10-Foot Supersonic Wind Tunnel at Mach 2.5 and a Reynolds number of 2.5×10^6 per foot (8.2×10^6/m). In addition to the flow surveys, measurements were made of the inlet and bleed flow rates, total-pressure recovery, and engine-face distortion. The maximum angle of attack before an inlet unstart was determined for critical and supercritical inlet operation. The effect of an overboard bypass system was also evaluated.

SYMBOLS

A	flow area, ft^2; m^2
A_c	capture area, 1.8916 ft^2; 0.1757 m^2
H	annulus height at local diffuser station, ft; m
h	distance from centerbody surface, ft; m
M	Mach number
m/m_0	mass-flow ratio
P	total pressure, lb/ft^2; N/m^2
ΔP	fluctuating component of total pressure, lb/ft^2; N/m^2

p	static pressure, lb/ft^2; N/m^2
R	inlet capture radius, 9.312 in.; 0.2365 m
r	radius, ft; m
S	centerbody bleed slot height, ft; m
T	total temperature, ^oR; K
W	weight flow rate, lb/sec; kg/sec
$W\sqrt{\theta}/\delta$	engine-corrected airflow, lb/sec; kg/sec
α	angle of attack, deg
θ	$T/519^o$ R; T/288.2 K
θ_l	cowl-lip-position parameter, $\tan^{-1}[1/(x/R)]$
δ	$P/2116$ lb/ft^2; $P/(10.13\times10^4$ $N/m^2)$
φ	total rake position, deg

Subscripts:

av	average
bl	bleed
by	bypass
l	centerbody bleed slot lip
max	maximum
min	minimum
rms	root-mean-square value
s	spike centerbody
t	throat
x	local
0	free stream
5	diffuser exit station

APPARATUS AND PROCEDURE

To simplify the mechanical design of the test inlet, the contraction ratio was varied with centerbody translation rather than by collapsing the second cone. At the design

Mach number of 2.5, 60 percent of the supersonic flow area contraction was external and 40 percent was internal. The inlet was attached to a cylindrical nacelle 25 inches (0.635 m) in diameter in which a J85-13 engine or a coldpipe choked-exit plug assembly could be installed. For this study, only the coldpipe was used. Figure 1(a) shows the inlet-nacelle combination mounted from a vertical strut in the wind tunnel test section. Figure 1(b) is an isometric view of the inlet.

At the design Mach number of 2.50 and a free-stream temperature of 702° R (390 K), the inlet was sized to match J85-13-engine-corrected airflow requirements of 34.89 pounds per second (15.83 kg/sec) with 88.6 percent of the capture mass flow at a total-pressure recovery of 0.90. This required an inlet capture area of 1.893 square feet (0.1758 m^2). Of the remaining inlet flow, 6 to 7 percent was allotted for performance bleed; 4 percent for engine cooling air; and the rest for overboard bypass flow, which was varied for terminal shock position control. Total-pressure distortion at the engine face of 0.10 or less was desired at the design conditions.

The essential features of the inlet were a bicone centerbody of 10° and 18.5° half-angle cones, and an initial internal cowl angle of 5° (fig. 1(c)). The internal oblique shock eminating from the cowl lip was cancelled at the centerbody impingement point. The remaining compression of the flow to a throat Mach number of 1.3 was isentropic. The oblique shock from the cowl lip and the isentropic compression fan from the cowl were focused at one point on the centerbody.

The supersonic portion of the inlet was designed with the aid of a preliminary computer program that employed the method of characteristics. However, a routine in this preliminary program, which was used to determine the second-cone shock position, did not converge properly. This predicted a shock position that was too far upstream and that resulted in a slightly imperfect inlet design. All experimental results for this report were obtained with this inlet. Subsequently, the improved characteristic program of reference 5 became available. The solution for the desired diffuser contours and flow properties using the program of reference 5 are shown in figure 2. This program was also used to recompute the flow field of the original design, and the displacement of the second shock is apparent in figure 3. For the design θ_l of the original inlet, 25.28°, the second-cone shock was to intersect the cowl lip but instead (as shown in fig. 3(a)) fell inside the cowl lip. Because of this error the oblique shock from the cowl lip interferes with the focused isentropic compression near the centerbody focal point. A stronger shock loss results from this focal point interference, which thereby lowers the pressure recovery near the spike surface. The oblique-shock-impingement and focused-compression point falls downstream of the centerbody slot lip, and the expansion of the flow that results from this slot will move the compression fan focal point even further downstream. Therefore, the shock cancellation criterion at the centerbody was not met.

In figure 3(b) the centerbody is translated to a θ_l position of 24.85° so that the second oblique shock would intersect the cowl lip. This translation of the centerbody corrects the interference of the oblique shock with the isentropic compression, but the compression-fan focal point still lies slightly rearward of the centerbody bleed lip. The data throughout the report reflect this result. If the compression fan were distributed on the centerbody over a short distance downstream of the cowl shock intersection point, the inlet would be less sensitive to errors of this type than it is when the focused-compression technique is employed. The coordinates of the actual centerbody and cowl are listed in table I.

The subsonic diffuser consisted of an initial throat region four hydraulic radii in length with a 1° equivalent conical expansion followed by the main diffuser. The diffuser just downstream of the throat was mated to an existing subsonic diffuser described in references 2 and 3. Since the throat of the present inlet had a larger radius than the throat of the reference 2 inlet, a relatively sharp curve in the cowl contour occurred at the diffuser mating location. The overall design length from cone tip to compressor face was 7.26 cowl-lip radii. Figure 4(a) shows the internal area distribution through the inlet for a cowl-lip-position parameter of 25°. Provisions were included for installing vortex generators on the cowl and the centerbody aft of the throat region at an x/R of 3.66. Details of the vortex generator design are shown in figure 4(b). Inlet configurations using vortex generators are identified herein as shown in the figure.

The aft portion of the subsonic diffuser contained three hollow centerbody support struts which divided the duct into three compartments back to the engine face. The inlet diffuser also included two bypass systems: a high-response overboard system for shock position control, and a low-speed valve to control secondary flow through the nacelle for engine cooling. Both systems were sealed for the bleed study and opened for the overall performance study presented in this report. The duct entrance into the bypass plenum was modified to minimize resonance by the installation of louvered segments, as discussed in reference 6.

To minimize the shock boundary layer interaction in the throat region, a porous bleed region was designed into the cowl and a flush slot was located ahead of the centerbody break. The porous bleed on the cowl consisted of nine rows of 0.125-inch (0.3175 cm) diameter holes equally spaced per row. The rows were alternately staggered to obtain maximum area coverage. The cowl bleed pattern is shown in figure 5(a) and the centerbody bleed slot is described in figure 5(b). From the cowl hole pattern it can be seen that two full rows of holes are required to bleed the full cowl perimeter without leaving gaps. The porous bleed pattern could be varied by filling selected holes. The four bleed patterns considered in this study are shown in figures 5(a) and (b). The first configuration, M-1, provided for large amounts of bleed flow on the centerbody and on the cowl, forward and aft of the geometric throat. For configuration M-2, the

porous bleed area on the cowl was reduced by one-half with about 30-percent area reduction on the centerbody. The M-3CB configuration maintained the same bleed area on the cowl and centerbody as configuration M-2, but the forward cowl bleed pattern was moved two rows aft. Vortex generators were installed on the centerbody of configuration M-3CB. For configuration M-4 and M-4CCB the aft bleed of configuration M-3CB was sealed. Configuration M-4 had no vortex generators and configuration M-4CCB had vortex generators installed on both the centerbody and cowl. The flush slot bleed on the centerbody was located ahead of the cowl shock, as in reference 7. Two flush slot configurations were studied and are defined in figure 5(b).

The cowl bleed flow was discharged overboard through an exit shown in figure 6(a). The exit has a 20° discharge angle relative to the external surface. The centerbody bleed flows into one plenum and is then ducted through the hollow centerbody support struts to 30° louvered exits. All exit areas were sized large enough to ensure choking of the bleed holes.

Boundary layer properties were investigated on the cowl and centerbody by total-pressure-tube rakes at the throat (station 2, fig. 6(a)). Rakes in the subsonic diffuser aft of the throat region (station 3), at the subsonic diffuser midpoint (station 4) and at the diffuser exit (station 5) were used to determine local flow profiles. The rakes were circumferentially indexed to avoid mutual interference effects. Details of the total-pressure rakes are shown in figure 6(b).

Figure 6(c) shows the compressor-face, steady-state pressure instrumentation (station 5). The overall diffuser-exit, total-pressure recovery was determined from rakes 1 to 6, which were area weighted. The additional measurement by rake 7 was included in the distortion calculations and in the duct local flow profile. Static-pressure distribution along the top centerline of both the cowl and centerbody was also measured. The static tube locations along the cowl and centerbody are presented in table II.

In order to measure the fluctuating component of total pressure, subminiature absolute pressure transducers were mounted in rotating rakes. These rakes were cantilevered from the centerbody in both the top and lower left duct segments. An assumption was made that the pressures in the lower left segment were similar to the pressures in the lower right segment. The total-pressure transducer was mounted tangential to the tube to protect the transducer diaphragm from particle damage. The 0.75-inch (1.905 cm) tube length was necessary to obtain an accurate total pressure but still was short enough to yield a flat response to at least 1000 hertz. The output signals of the rotating rake transducers were filtered by first-order, low-pass filters with a 1000-hertz corner frequency and measured with true rms meters. Further details of the response characteristics of the transducer-tube apparatus are given in reference 8.

At each steady-state operating condition, dynamic data were recorded at the four rotating rake positions shown in figure 6(d). The average value of the 16 rms measure-

ments of the fluctuating component of total pressure in each segment was ratioed to the average steady-state recovery pressure. The final average value was obtained by adding one-third of the top segment value to two-thirds of the lower left segment value. This final average value is defined as the dynamic distortion level for that particular operating condition.

RESULTS AND DISCUSSION

The results of this investigation are discussed in two parts: first, the effect of performance-bleed quantity and location on inlet performance; and second, the overall inlet performance characteristics with operating bypasses.

Performance Bleed

The effect of the various bleed configurations on peak inlet performance with variation of the cowl-lip-position parameter θ_l is shown in figure 7. All three configurations show little variation in peak total-pressure recovery as centerbody position is changed, with the M-2 configuration being least sensitive. As expected, configuration M-1 (with twice the porous cowl area of the other configurations) shows almost twice the amount of bleed mass flow over the range of cowl-lip-position parameter values. An increase in the steady-state distortion was observed when the performance bleed area of configuration M-1 was reduced to that of configuration M-2. A combination of relocating the forward cowl bleed and adding vortex generators on the centerbody, as in configuration M-3CB, reduced the distortion significantly.

The overall performance of the three inlet configurations is presented in figure 8. The cowl-lip-position parameter for configuration M-1 is 25.14° (capture mass-flow ratio of 1.00), and for configurations M-2 and M-3CB is 25.00° (capture mass-flow ratio of 0.995). These positions correspond to the highest recovery points of figure 7. The supercritical bleed mass flow for configuration M-1 was about 0.054, while that of configurations M-2 and M-3CB was about 0.032. In spite of the reduced bleed for configuration M-2, the pressure recovery at critical inlet operation (terminal shock at geometrical throat) was the same value of 0.879 as for configuration M-1. The unusual shape of the distortion curve can be correlated with supersonic flow distortion at supercritical shock positions. However, at critical operation the distortion of 0.185 was also unchanged by changing the bleed from configuration M-1 to M-2. The high level of distortion at critical operation was probably a result of improper control of the flow-field focal point on the centerbody. This results in distorted supersonic flow in the throat

and contributes to the compressor-face distortion for critical and supercritical conditions. This is shown later in figure 11. Use of vortex generators on the centerbody (configuration M-3CB) substantially reduced the distortion level to 0.130 at critical inlet operation. A slight increase in pressure recovery to 0.884 was also observed for configuration M-3CB for this operating condition.

The subcritical operating range between critical and peak performance conditions for configuration M-1 was about 4.6 percent in terms of engine-corrected airflow (fig. 8(a)). Configurations M-2 and M-3CB show only about 1.5-percent subcritical operating range. The larger stable range of configuration M-1 was due primarily to the larger bleed capacity on the cowl surface.

Variation of the cowl and centerbody bleed flows with overall pressure recovery is shown in figure 9. The supercritical bleed flows for configurations M-2 and M-3CB are identical on the cowl and centerbody. Configuration M-3CB shows slightly larger cowl bleed flows at the peak conditions.

The variation in bleed plenum pressure recovery in the cowl and centerbody with bleed mass flow is shown in figure 10. The exit area was large enough to maintain the bleed holes in a choked condition.

Local total-pressure profiles at various stations in the diffuser are presented in figure 11 for both peak and critical operation. At peak operating conditions, the cowl boundary layer at station 2 was well behaved. This profile was the same for critical inlet operation. The total-pressure profiles on the centerbody at the throat region show that for configuration M-1, the focused isentropic compression coalesces with the cowl shock above the centerbody, but ahead of the bleed lip, for both peak and critical operation (see fig. 3). For the θ_l position 25.00° the cowl shock crosses the throat rake for configurations M-2 and M-3CB. This is shown by the lower pressure measured at a throat height ratio of about 0.10. As explained earlier in the section APPARATUS AND PROCEDURE, due to a computer program error, the design did not meet the requirement for cowl shock impingement and cancellation at the spike shoulder.

At the throat exit station, the total-pressure profiles near the cowl show that the cowl bleed of configuration M-1 completely removed the boundary layer. For critical operation, little variation of the pressure profile near the cowl surface is shown for all three configurations. At the throat exit for peak conditions (fig. 11(a)), a good total-pressure profile is evident except at the centerbody. At critical conditions (fig. 11(b)), the throat profile is somewhat distorted for configurations M-2 and M-3CB, showing the effect of throat supersonic flow distortion.

The results of improper control of the flow on the centerbody are clearly shown in the throat exit profiles and all the way downstream to the compressor face. The effect of vortex generators on the centerbody flow of configuration M-3CB for peak and critical operation is clearly seen at the mid-diffuser and compressor-face rake stations.

The cowl and centerbody static-pressure distributions for all three configurations are presented for critical operation in figure 12 and for peak operation in figure 13. At critical inlet operation, the static-pressure profiles are nearly equal for all three configurations (fig. 12). At peak inlet operation, the terminal shock for configuration M-1 approaches a plane wave at the edge of the centerbody bleed slot. The large bleed on the cowl and centerbody are responsible for this condition. With the reduced bleeds of configurations M-2 and M-3CB the terminal shock does not attain this forward position.

The inlet performance through an angle-of-attack range is presented in figure 14. The following procedure was used to obtain the angle-of-attack data. For maximum angle of attack at critical inlet operation: (1) the inlet was set at critical for 0° angle of attack; and (2) the model angle of attack was increased until an unstart occurred. Data were recorded for an angle slightly less than the unstart angle of attack.

For maximum angle of attack at supercritical inlet operation: (1) the inlet mass-flow plug was fully retracted, (2) the model angle of attack was increased until an unstart occurred, (3) the inlet was restarted and the model angle of attack was set slightly less than the unstart angle, (4) the mass-flow plug was then closed until the inlet unstarted, (5) after the inlet was restarted, the plug was relocated near the position causing unstart. This data point is defined as the peak recovery at that condition. At the angles of attack less than maximum, just the peak pressure recovery condition was determined. All data presented in figure 14 are for these peak pressure recovery conditions.

In general, large angle-of-attack variation was exhibited by all three inlet configurations. A maximum angle of attack of 9.4° was obtained by configuration M-1 before the inlet unstarted. Configurations M-2 and M-3CB showed maximum angles of attack of about 8.5°. The maximum angles of attack obtained when the inlet is at critical operation are indicated by the flagged symbols on figure 14. Configuration M-1 shows 6.4° angle of attack, while configuration M-2 has 4.1° and configuration M-3CB has 4.8° angle-of-attack capability for critical inlet operation.

All three configurations show a slight increase in the distortion level to about 4°. Configuration M-2 exhibits the largest distortion of about 0.19 at 4° angle of attack, while configurations M-1 and M-3CB show only about 0.16. Rapid increases in distortion levels are observed for all three configurations for angles of attack greater than 5°.

The effect of angle of attack on compressor-face, total-pressure profiles for the three inlet configurations is shown in figure 15. The inlet operating conditions presented are (1) critical inlet operation at 0° angle of attack, (2) maximum angle of attack for critical inlet operation, and (3) peak recovery at maximum angle of attack for supercritical operation before an inlet unstart. All configurations show deterioration of the compressor-face flow at rakes 1, 2, 3, and 4 as the angle of attack is increased. At

the high angles of attack the inlet flow is washed around the centerbody, resulting in high energy flow into the top segment of the duct.

Figure 16 shows the static-pressure distributions for angle-of-attack operation of the three inlet configurations.

Schlieren photographs of the shock patterns of the inlet at the various angles of attack are shown in figure 17. Figure 17(a) shows the highest angle of attack, 9.4°, obtained with configuration M-1. Figures 17(b) to (e) present the shock patterns at the various angles of attack for configuration M-3CB.

Limited data were taken at a reduced free-stream Mach number of 2.4. The data showed that for configuration M-3CB, the inlet remained started at the cowl-lip-position parameter of 25.00°. This would indicate an inlet Mach number tolerance of at least 0.10.

Inlet Operation With Bypass Flow

All the data presented in this section were taken with the overboard and ejector bypass systems operating. The bypass system is the same as in reference 3.

Reference 3 shows that the total-pressure profiles on the cowl were improved when the inlet bypass systems were operating. Therefore, an effort was made in the present study to further reduce the bleed mass flow by relying on vortex generators (on the cowl and centerbody) and on bypass flow to help maintain reasonable distortions. The overall inlet performance with vortex generators (configuration M-4CCB) and without vortex generators (configuration M-4) was determined and the results are presented in figure 18. The inlet performance of configuration M-4 is shown in figure 18(a). At the critical operating condition the pressure recovery was 0.890 with steady-state distortion of 0.157. The peak pressure recovery obtained for this configuration was 0.900. The dynamic distortion near critical operation indicates reasonable values, even at angle of attack. However, the steady-state distortions appear high enough to possibly prevent stable engine operation.

The inlet performance of configuration M-4CCB is shown in figure 18(b). A peak pressure recovery of 0.915 with 0.063 distortion was obtained with this configuration. At critical inlet operation (presumed to be the engine match condition with $W\sqrt{\theta}/\delta$ = 35.5 lb/sec or 16.1 kg/sec), the pressure recovery was 0.885 with 0.033 bleed mass flow ratio. The steady-state distortion at the match point was about 0.045 and remained below a value of 0.125 for a large part of the inlet operating range. The capture mass-flow ratio was 0.995 and the supercritical bleed mass-flow ratio was 0.025 for this configuration. Bypass air accounted for the remainder of the capture mass flow. The effect of vortex generators in minimizing the dynamic distortion is shown in figure 18(b).

The value of dynamic distortion remained below 0.04 for all inlet operating conditions even at high angle-of-attack operation. The maximum angle of attack for critical inlet operation was 4.5° with a recovery of 0.865 and a steady-state distortion of 0.145. The maximum angle of attack for supercritical operation before inlet unstart was 8.2° with a steady-state distortion of 0.26 at peak recovery. As stated earlier the dynamic distortion at all angles of attack remained below 0.04, and at 4.5° angle of attack the level was about 0.01.

The cowl and centerbody static-pressure distributions along the top centerline are presented in figures 19 and 20. Static-pressure distributions for the various engine-corrected airflows are presented in figure 19. Distributions for operation along the match-corrected airflow line (with bypass door variation) are presented in figure 20.

The effect of vortex generators on the compressor-face, total-pressure profiles is shown in figure 21 by comparing data from configuration M-4 without generators to data from configuration M-4CCB with generators. At 0° angle of attack and critical inlet operation (fig. 21(a)), the vortex generators nearly eliminated the distortion without decreasing overall total-pressure recovery. These data show effects similar to those described in reference 9. The profiles for maximum angle of attack with critical inlet operation are shown in figure 21(b). The maximum angle of attack for critical operation was slightly greater when vortex generators were used. With the vortex generators, the distortion was significantly reduced, with very little sacrifice in overall total-pressure recovery. In the upper section of the duct (rakes 5, 6, and 7), the vortex generators provided more improvement in distortion characteristics than in the lower segments. At the maximum angle of attack for supercritical operation and peak recovery (fig. 21(c)), a significant difference between the flow in the upper section of the duct (rakes 5, 6, and 7) and that in the lower sections is evident from the total-pressure profiles. At this condition a sacrifice in total-pressure recovery was observed with the improved distortion. At the high angles of attack, the flow in the upper section of the duct has a compression and expansion region before the final terminal shock, similar to profiles shown in figure 16. The vortex generators are located in the expansion region. This would suggest that the vortex generators in the upper section of the duct are in supersonic flow which causes a larger drop in pressure recovery.

The overall performance of inlet configuration M-3CB is shown in figure 22. This configuration had vortex generators installed only on the centerbody. In this case an engine-corrected airflow of 34.5 pounds per second (15.65 kg/sec) was used as a match condition for the inlet. The inlet pressure recovery at this match condition was 0.903 with a bleed mass-flow ratio of 0.041 and corresponding steady-state distortion of 0.102. Bypass air accounted for the remainder of the capture mass flow. At the minimum stable or peak inlet operating condition, the recovery was 0.912 and the steady-state distortion was 0.113. This condition provided a stability range of 3.4 percent in terms

of engine-corrected airflow for this inlet. Increasing supercritical operation from the match condition resulted in a rapid increase of the steady-state distortion level. Supercritical operation to pressure recoveries of about 0.82 with the overboard bypass system resulted in higher distortion levels than when the engine airflow was varied. The dynamic distortion levels were less than 0.03 for as much as 10-percent supercritical operation.

The maximum angle of attack for critical inlet operation was 4.36°. The pressure recovery at this condition was 0.875 with a steady-state distortion level of 0.17. The maximum unstart angle of attack for supercritical operation was 8.88°. However, the steady-state distortion at this condition was very high at 0.42. In spite of the high steady-state distortions at angle of attack, the dynamic distortions remained at an acceptable level.

The solid circular symbol on figure 22 denotes an inlet unstarted but stable operating condition. If, during operation at the match condition, some perturbation should unstart the inlet, a stable inlet operation will occur without bypass or centerbody movement. The pressure recovery at this condition was 0.775 with a steady-state distortion level of 0.125. No dynamic distortion data were obtained for this unstarted condition.

A schlieren photograph showing the shock pattern for the unstarted but stable condition is shown in figure 23. This shows a third oblique shock from a centerbody boundary layer separation and the terminal shock, which combine with the two cone shocks to give good recovery.

Diffuser static-pressure distributions for various engine-corrected airflows are presented in figure 24. Diffuser static-pressure distributions for various bypass door settings at constant engine-corrected airflow are presented in figure 25. The position of the terminal shock in the throat region appears to move discontinuously through the throat region with small changes in diffuser backpressure. In order to provide more control of the terminal shock in the throat region, more bleed, judiciously located, would be needed, as in reference 3.

The effect of angle of attack on compressor-face, total-pressure profiles with bypass flow is presented in figure 26. At 0° and 4.36° angle-of-attack operation, the profiles are nearly the same except at the number 2 and number 3 rake positions in the lower part of the duct. At the higher angle of attack, 8.88°, large separated regions are observed in the lower two sections of the inlet duct.

Performance During Restart Cycle

Overall inlet pressure recovery and distortion during the restart cycle at a Mach number of 2.50 are shown in figure 27. Since the centerbody could not be collapsed to

restart the inlet, the centerbody was translated during the restart cycle. The data of figure 27 are plotted against the combined engine and overboard bypass mass flow. These data (other than started conditions at design θ_l) were obtained by varying the bypass with the exit plug set for engine-match airflow. The inlet was unstarted at the design spike setting by closing the overboard bypass doors. Immediately after unstart the external shock structure was unstable but could be stabilized by opening the overboard bypass doors. The minimum stable condition occurred at the same bypass door setting as for critical operation. This would indicate that no instability would persist if for some reason the inlet unstarted while at critical operation or at an engine-corrected airflow of 34.5 pounds per second (15.65 kg/sec). The minimum stable unstarted pressure recovery at design spike setting was 0.77 and remained within 1 percent of this value as the spike was extended to the restart position. Total-pressure distortions at these conditions varied between values of 0.11 and 0.14. Minimum stable started total-pressure recovery increased from 0.79 immediately after restart to 0.915 at the design spike position. Total-pressure distortions for these conditions also varied between values of 0.11 and 0.14. Cowl and centerbody static-pressure distributions corresponding to the data of figure 27 are presented in figures 28 and 29, respectively. These data, along with spike position, can provide representative pressure signals for bypass door position control during a restart cycle. With such a control, it should be possible to minimize the distortion and to maximize the pressure recovery during a restart cycle. In actual application to an aircraft, some combination of collapsing and translating the centerbody may be desirable to restart the inlet. The diffuser pressures then would differ from those shown.

Experimental and Predicted Restart Area Ratios

In a variable-geometry, mixed-compression inlet, the initial start or any restarts of supersonic flow in the inlet are usually accomplished by increasing the ratio of the throat area to the entering flow area. Mixed-compression inlets have been found to restart with less throat area than would be predicted from a one-dimensional flow analysis assuming uniform flow in front of a normal shock at the cowl lip. Reference 10 suggests a prediction technique based on measurements of flow separation within the unstarted flow field just before restart to determine the necessary contraction ratio to restart the inlet. Data for a Mach 3.0 inlet from reference 10, which was used to develop the prediction technique, are presented in figure 30. As shown, the inlet restarts well below normal shock values. Data are also presented for the actual and predicted restart contraction ratios for the present inlet and also for the inlet of reference 3. The inlet of reference 3 was designed for Mach 2.5 and employed 60-percent internal con-

traction. As shown, the predicted and actual contraction ratios for the present inlet and the inlet of reference 3 were similar. However, because of the increased amount of internal contraction for the inlet of reference 3, it required more spike translation than the present inlet (6 in. (15 cm) compared to 2 in. (5cm)) to obtain the contraction ratio needed for restart.

SUMMARY OF RESULTS

An investigation was conducted to determine the performance characteristics of an axisymmetric, bicone, mixed-compression inlet system designed for Mach 2.5 operation. Forty percent of the supersonic area contraction occurred internally. The internal compression was accomplished by the cowl-lip oblique shock and isentropic compression from the cowl, which were focused on the centerbody.

Data were obtained at a free-stream Mach number of 2.5 and Reynolds number of 2.5×10^6 per foot (8.2×10^6/m). Performance characteristics were obtained for various bleed configurations at (1) 0° angle of attack, (2) maximum angle of attack for critical inlet operation, and (3) maximum angle of attack before an inlet unstart occurred (supercritical operation). The following results were obtained:

1. Without the bypass system and with a supercritical performance bleed ratio of 0.032, a pressure recovery of 0.884 was attained at critical inlet operation. The distortion was about 0.185 but could be decreased to 0.135 with vortex generators on the centerbody. The maximum angle of attack before inlet unstart was 8.5° for supercritical operation and 4.8° for critical inlet operation. Higher angles (9.4°) could be obtained by increasing the supercritical bleed flow.

2. With centerbody vortex generators and an operating bypass system, the critical pressure recovery was increased to 0.903 and the distortion level was decreased to about 0.10. Dynamic distortion levels were 0.02 at critical operation and less than 0.03 even during supercritical operation. The maximum angle of attack at critical operation was 4.36° and the maximum angle before inlet unstart was 8.88°.

3. Further reduction of the performance bleed on the cowl and utilizing the inlet bypass system produced the following results: With vortex generators on the cowl and centerbody, the critical pressure recovery was 0.885 with a low distortion level of 0.045. Supercritical bleed mass-flow ratio was 0.025. Without vortex generators the critical pressure recovery stayed the same, but the distortion level increased to about 0.15. The maximum angle of attack at critical inlet operation was reduced from 4.5° to 4.0° when the vortex generators were eliminated.

4. During the inlet restart cycle, with inlet operation in the unstarted mode, the peak pressure recovery was about 0.78 over the range of cowl-lip-position parameters, and the distortion level varied between 0.10 and 0.14.

Lewis Research Center,
National Aeronautics and Space Administration,
Cleveland, Ohio, January 20, 1971,
720-03.

REFERENCES

1. Sorensen, Norman E.; Smeltzer, Donald B.: Investigation of a Large-Scale Mixed-Compression Axisymmetric Inlet System Capable of High Performance at Mach Numbers 0.6 to 3.0. NASA TM X-1507, 1968.
2. Cubbison, Robert W.; Meleason, Edward T.; and Johnson, David F.: Effect of Porous Bleed in a High-Performance Axisymmetric, Mixed-Compression Inlet at Mach 2.50. NASA TM X-1692, 1968.
3. Cubbison, Robert W.; Meleason, Edward T.; and Johnson, David F.: Performance Characteristics From Mach 2.58 to 1.98 of an Axisymmetric Mixed-Compression Inlet System With 60-Percent Internal Contraction. NASA TM X-1739, 1969.
4. Anderson, Warren E.; and Wong, Norman D.: An Experimental Investigation of a Two-Dimensional, Mixed-Compression, Variable-Geometry-Inlet System, I. Performance at Design Conditions, $M_\infty = 3.0$. TM X-2016, 1970.
5. Anderson, Bernhard H.: Design of Supersonic Inlets by a Computer Program Incorporating the Method of Characteristics. NASA TN D-4960, 1969.
6. Coltrin, Robert E.; and Calogeras, James E.: Supersonic Wind Tunnel Investigation of Inlet-Engine Compatibility. Paper 69-487, AIAA, June 1969.
7. Obery, Leonard J.; and Stitt, Leonard E.: Performance of External-Internal Compression Inlet With Abrupt Internal Turning at Mach Numbers 3.0 to 2.0. NACA RM E57H07a, 1957.
8. Calogeras, James E.: Experimental Investigation of Dynamic Distortion in a Mach 2.50 Inlet With 60-Percent Internal Contraction and Its Effect on Turbojet Stall Margin. NASA TM X-1842, 1969.
9. Mitchell, Glenn A.; and Davis, Ronald W.: Performance of Centerbody Vortex Generators in an Axisymmetric Mixed-Compression Inlet at Mach Numbers From 2.0 to 3.0. NASA TN D-4675, 1968.

10. Mitchell, Glenn A.; and Cubbison, Robert W.: An Experimental Investigation of the Restart Area Ratio of a Mach 3.0 Axisymmetric Mixed-Compression Inlet. NASA TM X-1547, 1968.

TABLE I. - INLET COORDINATES

(a) Centerbody.

x/R	r/R	x/R	r/R
0	0	4.500	0.4908
10° Conical section		4.550	.4823
1.0323	0.1820	4.600	.4735
18.5° Conical section		4.650	.4645
2.7751	0.7650	4.700	.4551
2.800	.7638	4.750	.4469
2.850	.7615	4.800	.4373
2.900	.7590	4.850	.4278
2.950	.7567	4.900	.4180
3.000	.7544	4.950	.4082
3.050	.7520	5.000	.3994
3.100	.7495	5.050	.3907
3.150	.7472	5.100	.3820
3.200	.7445	5.150	.3738
3.250	.7413	5.200	.3655
3.300	.7369	5.250	.3576
3.350	.7311	5.300	.3496
3.400	.7245	5.350	.3420
3.450	.7165	5.400	.3344
3.500	.7065	5.450	.3273
3.550	.6956	5.500	.3203
3.600	.6847	5.550	.3136
3.650	.6730	5.600	.3071
3.700	.6614	5.650	.2990
3.750	.6494	5.700	.2918
3.800	.6368	5.750	.2851
3.850	.6235	5.800	.2785
3.900	.6103	5.850	.2722
3.950	.5978	5.900	.2658
4.000	.5868	5.950	.2603
4.050	.5750	6.050	.2507
4.100	.5642	6.100	.2467
4.150	.5542	6.150	.2435
4.200	.5444	6.200	.2405
4.250	.5350	6.250	.2394
4.300	.5258	6.300	.2394
4.350	.5170	7.2411	.2394
4.400	.5080		
4.450	.4992		

(b) Cowl.

x/R	r/R	x/R	r/R	x/R	r/R
2.1167	1.0000	3.600	0.9559	5.150	0.9179
2.150	1.0028	3.650	.9514	5.200	↓
2.200	1.0073	3.700	.9470	5.250	↓
2.250	1.0113	3.750	.9426	5.300	↓
2.300	1.0148	3.800	.9384	5.350	↓
2.350	1.0171	3.850	.9343	5.400	↓
2.400	1.0181	3.900	.9302	5.450	↓
2.450	1.0181	3.950	.9264	5.530	↓
2.500	1.0165	4.000	.9226	Bypass gap	
2.550	1.0134	4.050	.9190	6.140	0.8868
2.600	1.0095	4.100	.9157	6.150	.8866
2.650	1.0056	4.150	.9126	6.200	.8856
2.700	1.0022	4.200	.9100	6.250	.8847
2.750	.9993	4.250	.9075	6.300	.8837
2.7751	.9982	4.300	.9057	6.350	.8825
2.800	.9971	4.350	.9046	6.400	.8809
2.850	.9952	4.400	.9044	6.450	.8786
2.900	.9935	4.450	.9048	6.500	.8762
2.950	.9920	4.500	.9057	6.550	.8736
3.000	.9906	4.550	.9071	6.600	.8711
3.050	.9893	4.600	.9086	6.650	.8678
3.100	.9880	4.650	.9102	6.700	.8654
3.150	.9870	4.700	.9117	6.750	.8640
3.200	.9857	4.750	.9131	6.800	.8632
3.250	.9841	4.800	.9144	6.850	.8627
3.300	.9820	4.850	.9156	6.900	.8624
3.350	.9791	4.900	.9166	6.950	.8621
3.400	.9755	4.950	.9173	7.2411	.8621
3.450	.9706	5.000	.9178		
3.500	.9654	5.050	.9179		
3.550	.9605	5.100	.9179		

TABLE II. - STATIC-PRESSURE-

TAP LOCATIONS

Cowl statics (top centerline), x/R	Centerbody statics (top centerline), x/R
2.252	0.752
2.305	.859
2.359	.899
2.413	.967
2.466	1.074
2.520	1.181
2.574	1.289
2.627	1.503
2.681	1.665
2.748	1.879
2.802	2.094
2.856	2.309
2.909	2.470
2.936	2.604
2.976	2.671
3.030	2.687
3.070	2.792
3.111	2.859
3.151	2.913
3.218	2.940
3.304	2.980
3.433	3.034
3.809	3.074
3.970	3.114
4.131	3.155
4.583	3.249
4.884	3.329
5.475	3.396
6.280	3.463
6.666	3.732
	3.866
	3.973
	4.583
	6.666

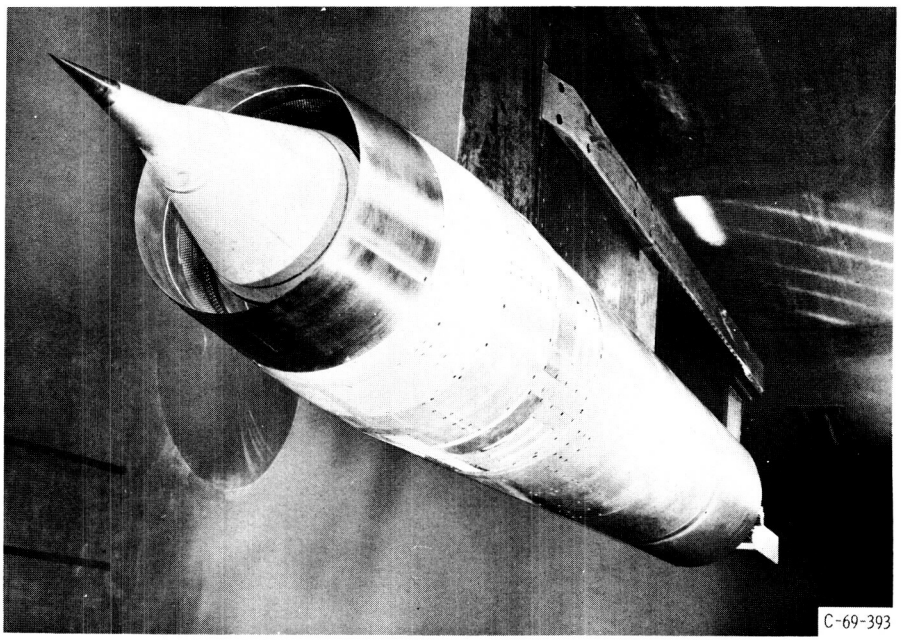

(a) Model installed in 10- by 10-foot Supersonic Wind Tunnel.

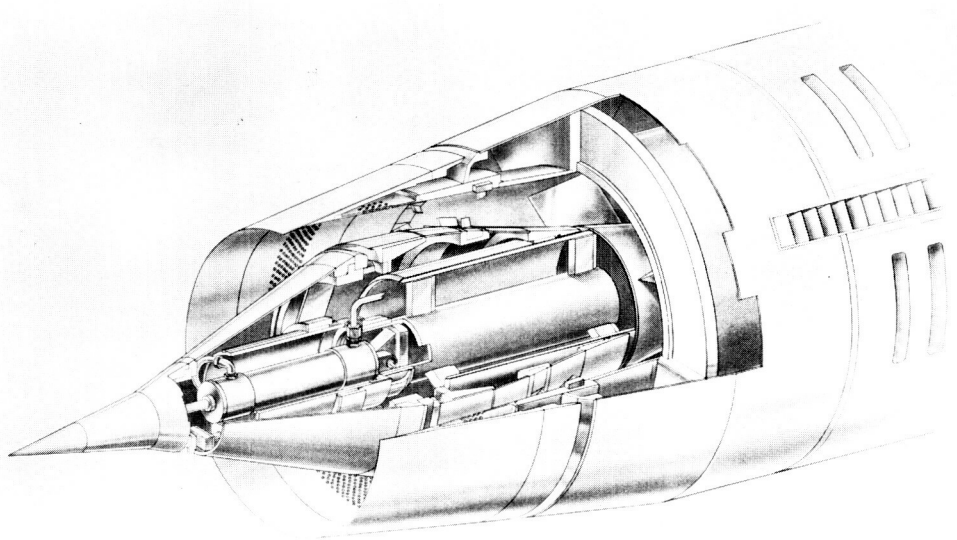

(b) Isometric view of model.

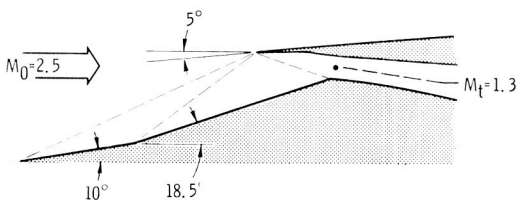

(c) Sketch of mouel.

Figure 1. - Focused-compression inlet.

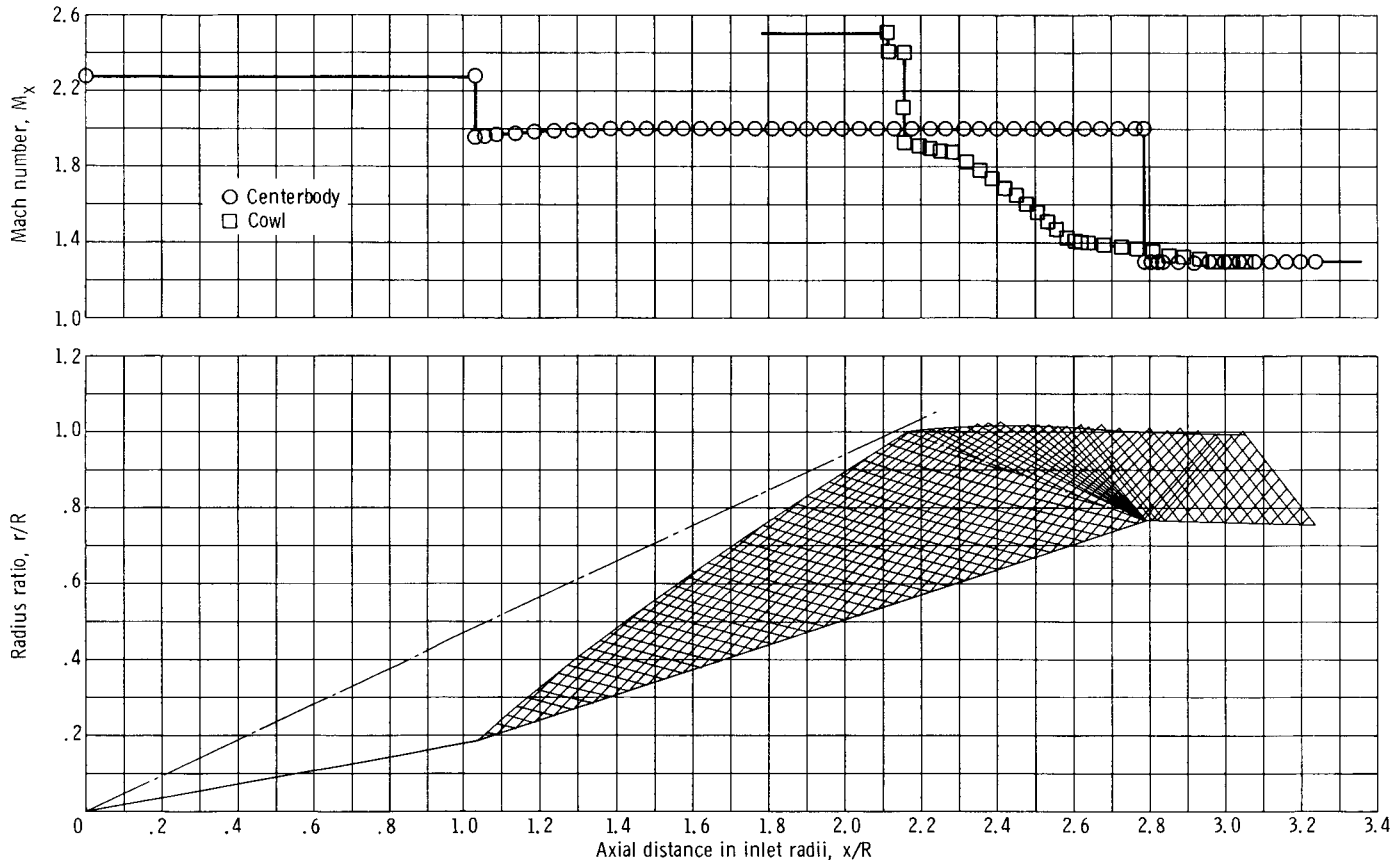

Figure 2. - Characteristic solution.

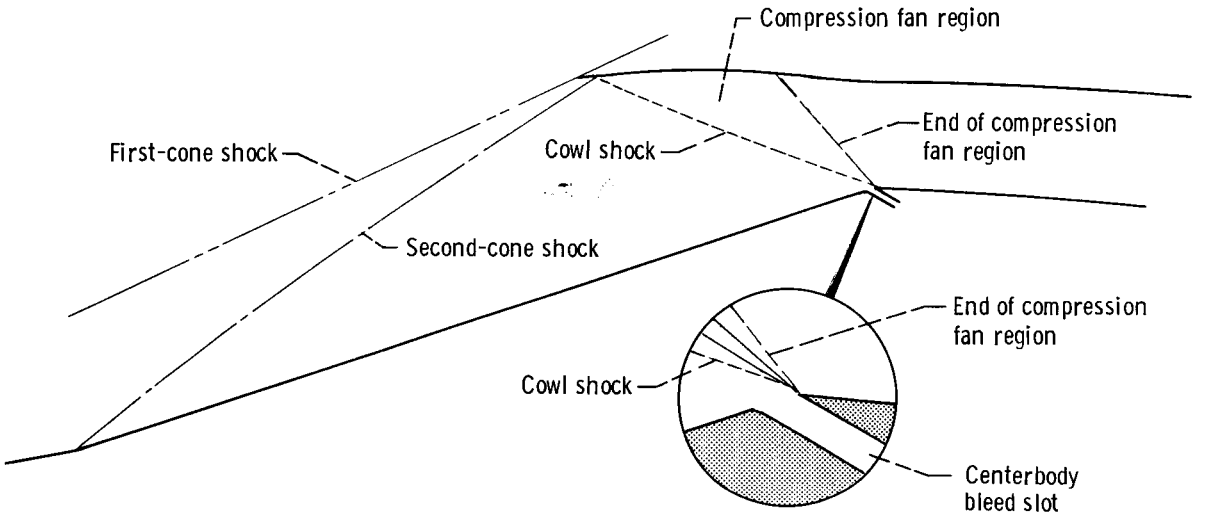

(a) Original design position; θ_l=25.28°.

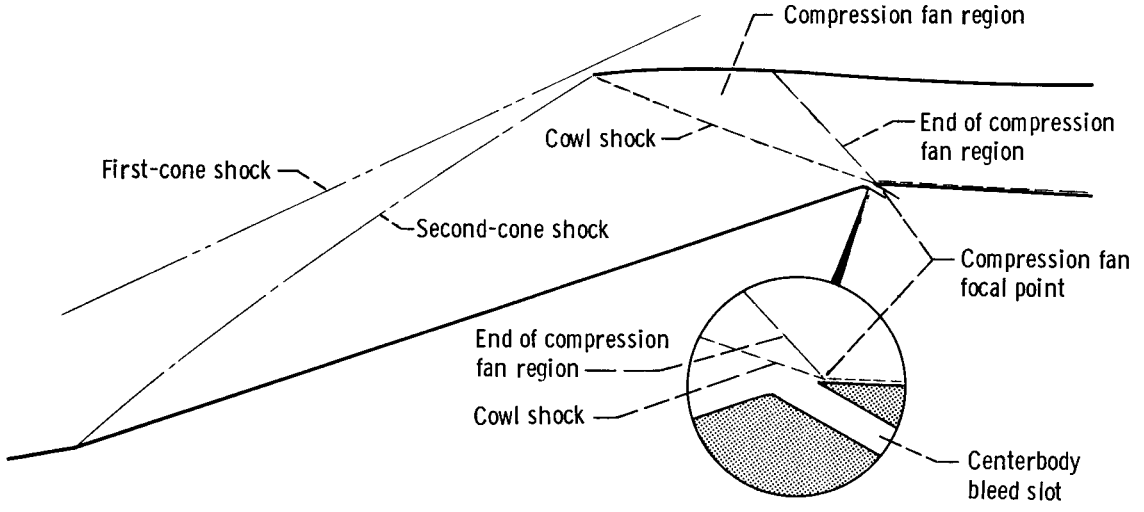

(b) Centerbody translated position; θ_l=24.85°.

Figure 3. - Comparison of inlet contour with characteristic solution, at different values of cowl-lip-position parameter θ_l.

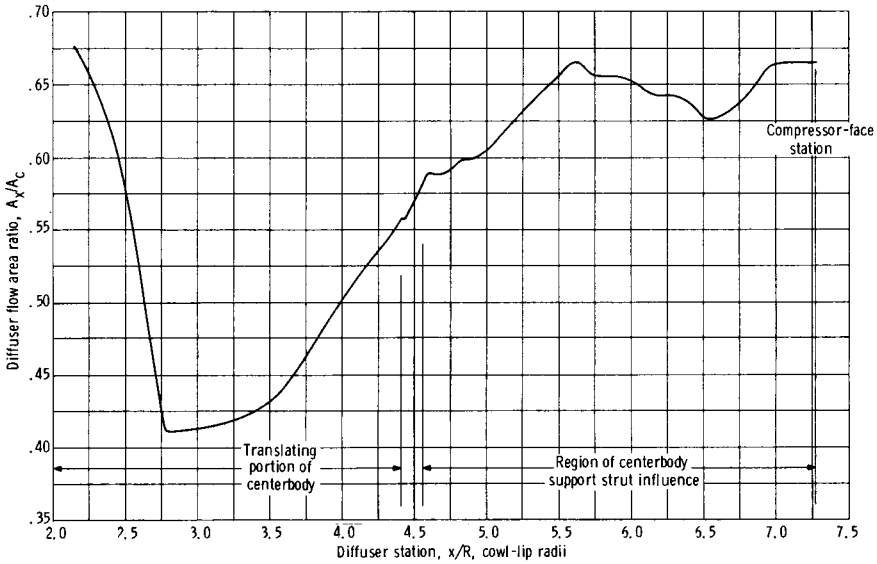

(a) Diffuser area variation; cowl-lip-position parameter, $\theta_L = 25.00^0$.

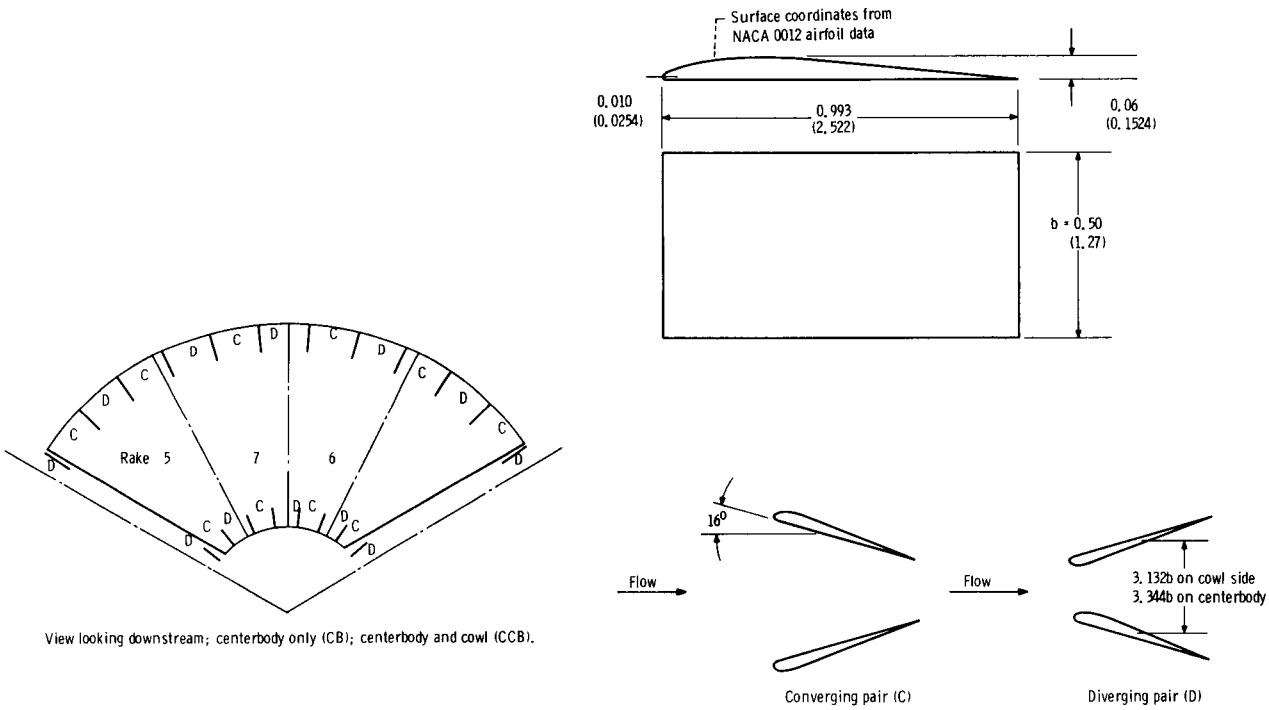

View looking downstream; centerbody only (CB); centerbody and cowl (CCB).

(b) Vortex generator design.

Figure 4. - Diffuser details. Dimensions in inches (centimeters).

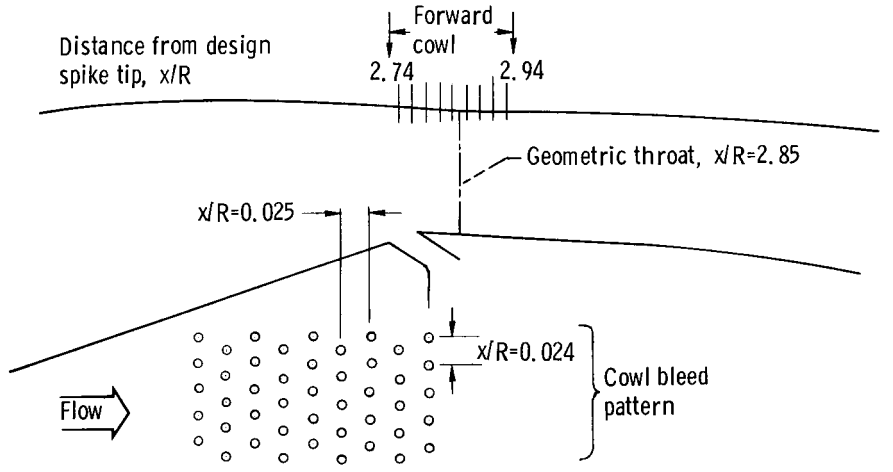

Configuration	○ Row opened ● Row closed ◑ Alternate holes open	Centerbody bleed configuration	Vortex generators
M-1	○ ○ ○ ● ● ● ● ○ ○	MS-1	None
M-2	○ ◑ ● ● ● ● ◑ ● ◑	MS-2	None
M-3CB	● ● ○ ◑ ● ● ◑ ● ◑	MS-2	Centerbody
M-4	● ● ○ ◑ ● ● ● ● ●	MS-2	None
M-4CCB	● ● ○ ◑ ● ● ● ● ●	MS-2	Cowl and centerbody

(a) Cowl bleed.

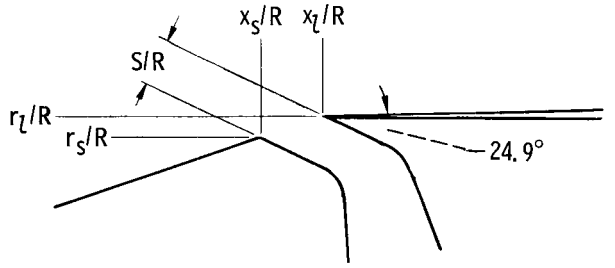

Centerbody slot bleed

Centerbody bleed configuration	x_s/R	x_l/R	r_s/R	r_l/R	S/R
MS-1	2.729	2.776	0.749	0.7645	0.0376
MS-2	2.741	2.776	.753	.7645	.0258

(b) Centerbody bleed configurations.

Figure 5. - Performance bleed configuration.

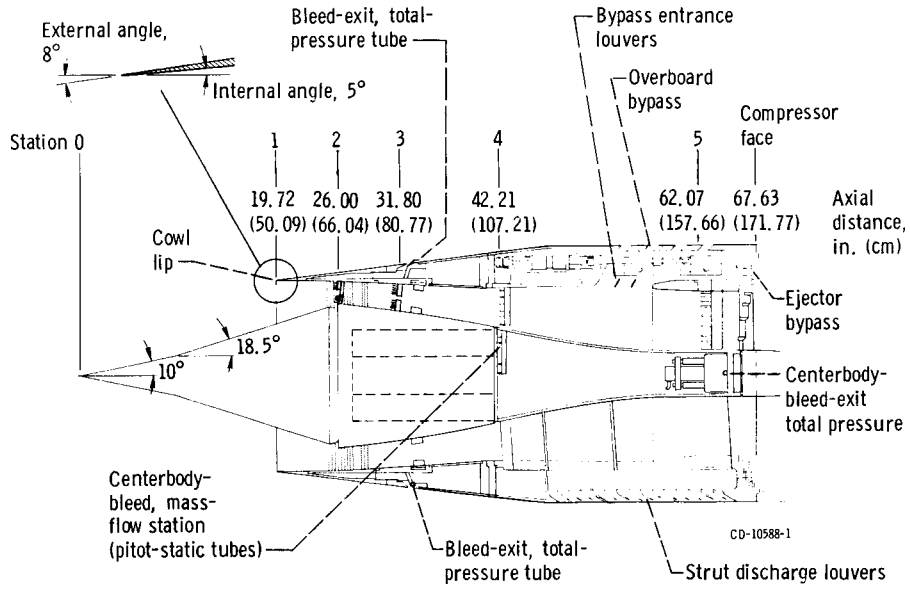

(a) Total-pressure-tube rake locations.

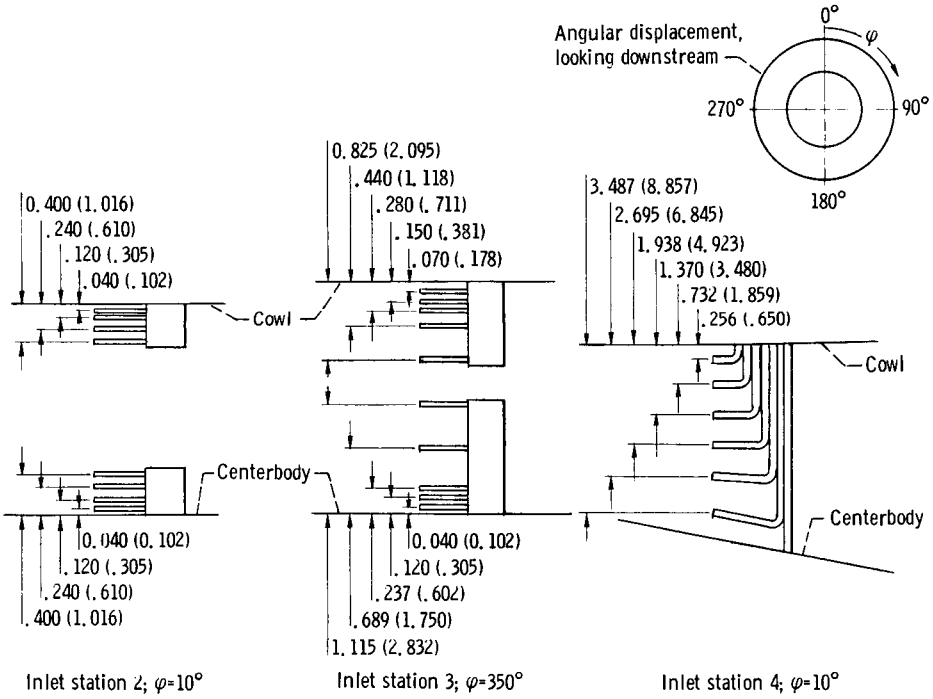

(b) Diffuser total-pressure rakes, at total rake positions φ.

Figure 6. - Pressure instrumentation. All dimensions in inches (cm).

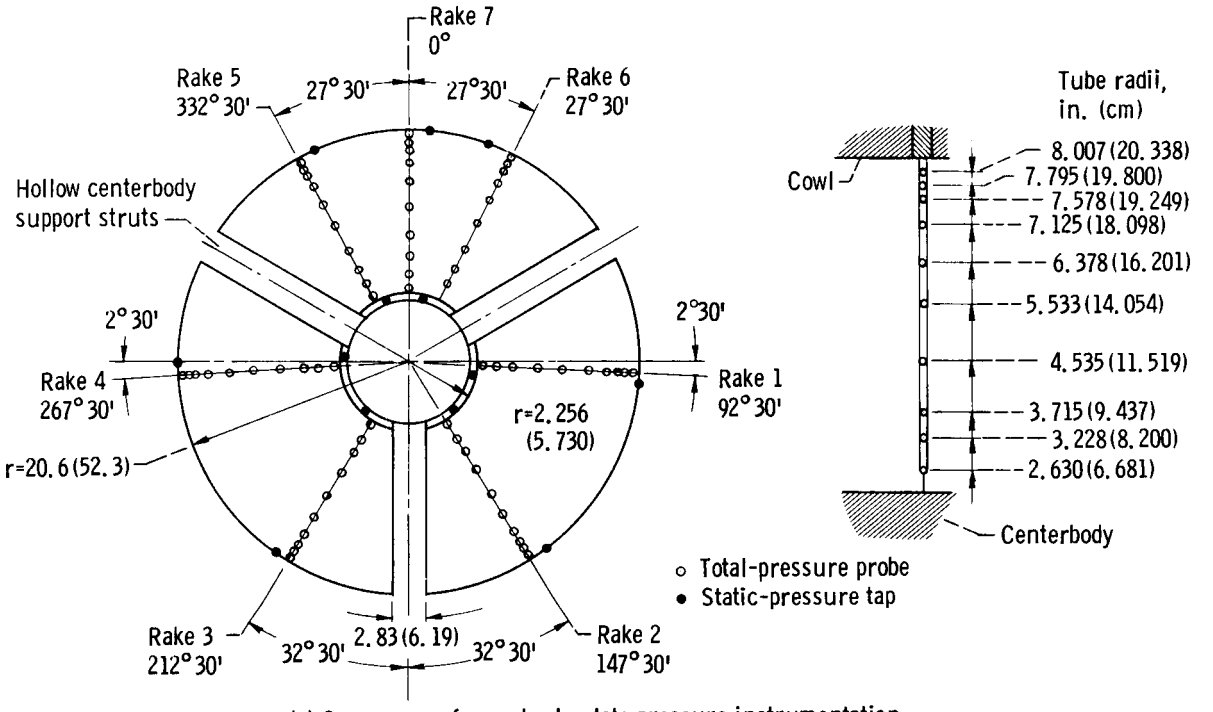

(c) Compressor-face, steady-state pressure instrumentation.

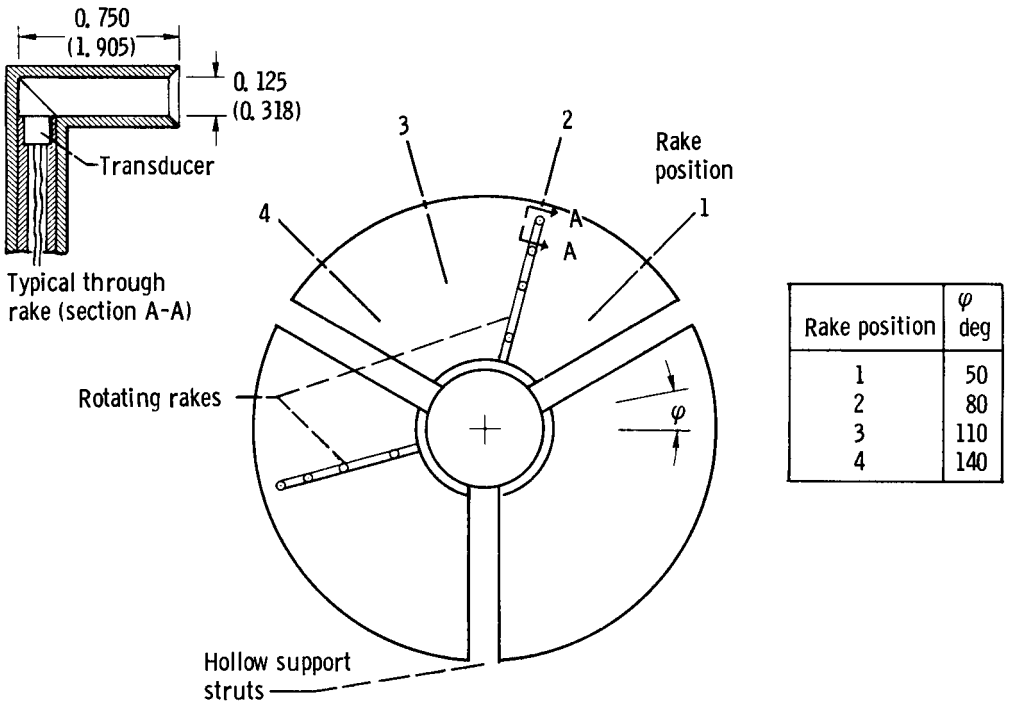

Rake position	φ deg
1	50
2	80
3	110
4	140

(d) Compressor-face dynamic instrumentation.

Figure 6. - Concluded.

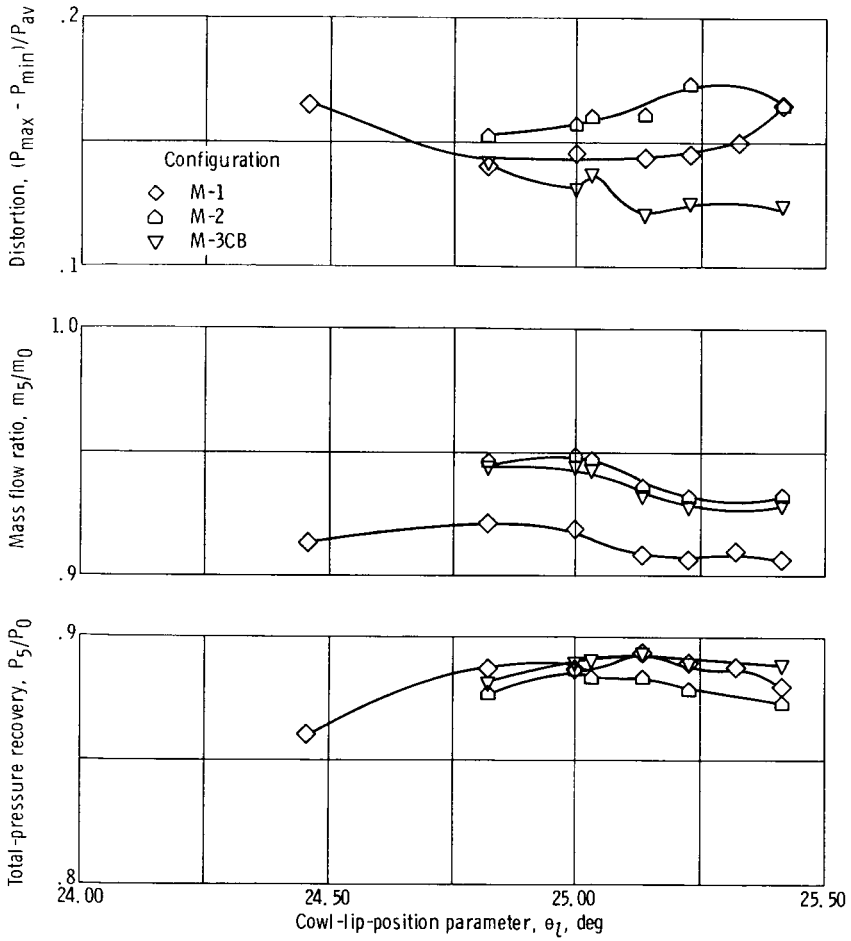

Figure 7. - Effect of spike position on peak inlet performance for various bleed locations. Angle of attack, 0^0.

Solid symbols denote inlet buzz
Half-closed symbols denote unstarted but stable operation
Tailed symbols denote critical operation

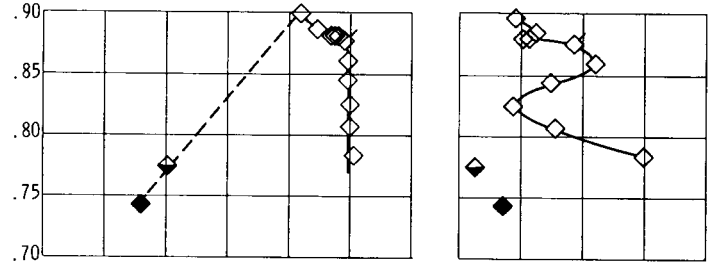

(a) Bleed configuration M-1; cowl-lip-position parameter, 25.14^0.

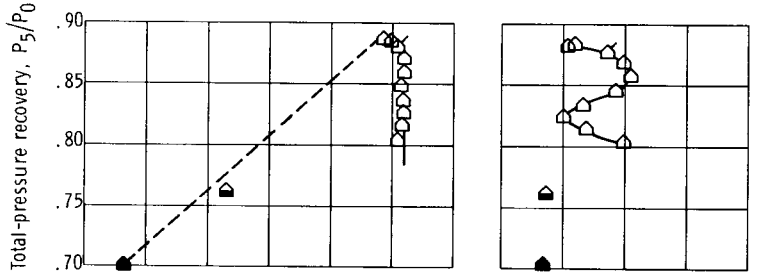

(b) Bleed configuration M-2; cowl-lip-position parameter, 25.00^0.

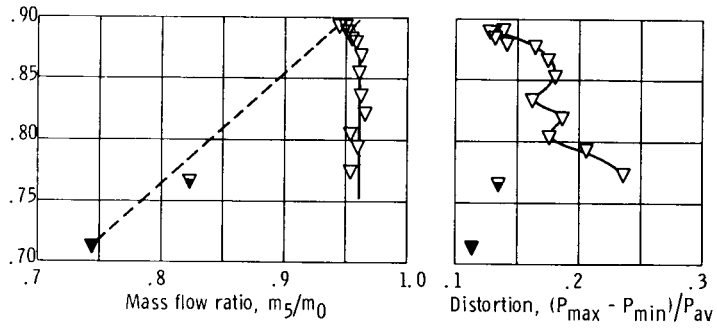

(c) Bleed configuration M-3CB; cowl-lip-position parameter, 25.00^0.

Figure 8. - Effect of bleed location on overall inlet performance. Angle of attack, 0^0.

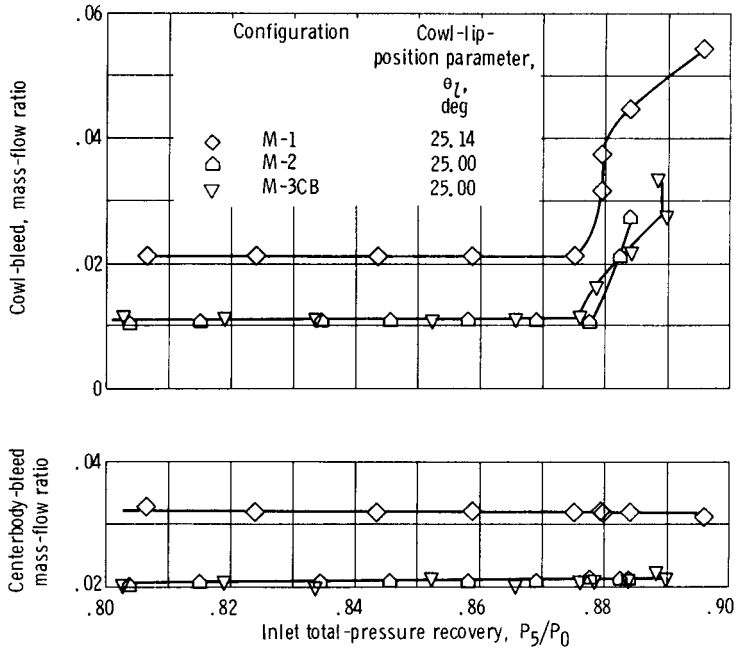

Figure 9. - Variation of bleed flow with overall inlet recovery. Angle of attack, 0^0.

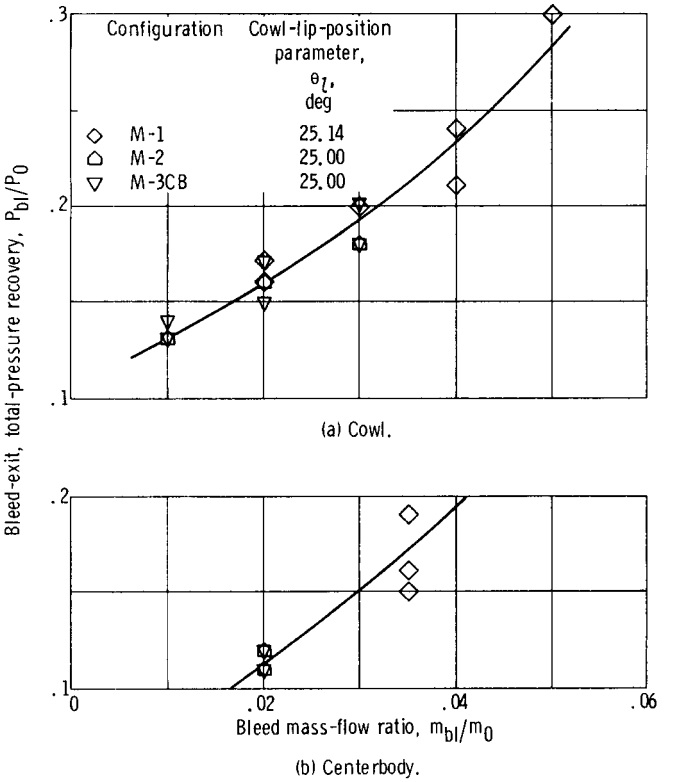

(a) Cowl.

(b) Centerbody.

Figure 10. - Variation of bleed-exit pressure recovery with bleed mass flow. Angle of attack, 0^0.

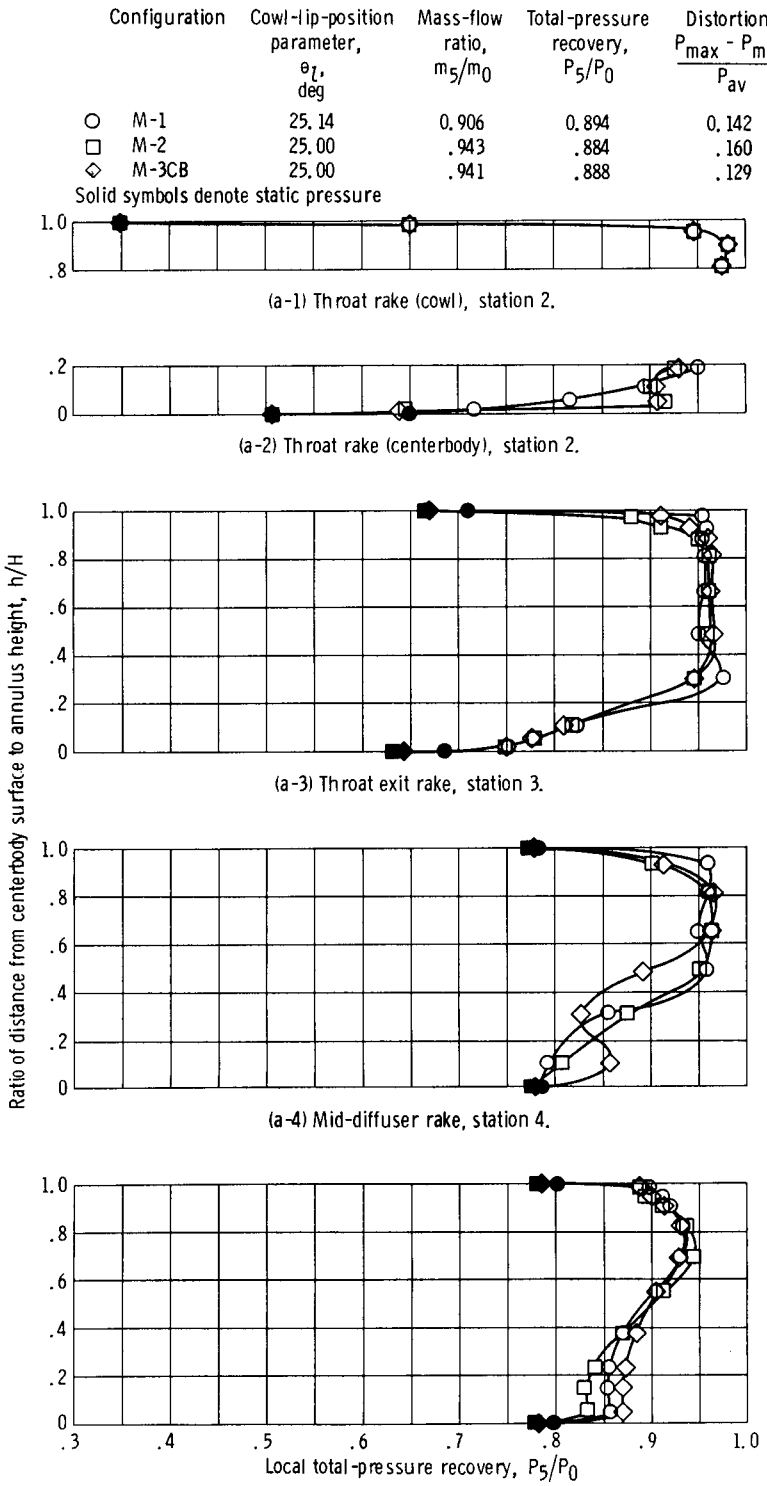

(a-1) Throat rake (cowl), station 2.

(a-2) Throat rake (centerbody), station 2.

(a-3) Throat exit rake, station 3.

(a-4) Mid-diffuser rake, station 4.

(a-5) Diffuser-exit station, rake 7, station 5.

(a) Peak inlet operating conditions.

Figure 11. - Effect of bleed location on diffuser performance. Angle of attack, 0^0.

Configuration		Cowl-lip-position parameter, θ_l, deg	Mass-flow ratio, m_5/m_0	Total-pressure recovery, P_5/P_0	Distortion, $\frac{P_{max} - P_{min}}{P_{av}}$
○	M-1	25.14	0.933	0.879	0.152
□	M-2	25.00	.951	.878	.169
◇	M-3CB	25.00	.951	.884	.132

Solid symbols denote static pressure

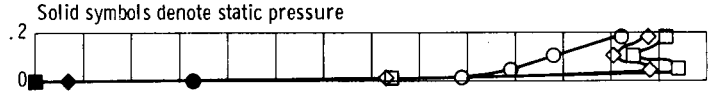

(b-1) Throat rake (centerbody), station 2.

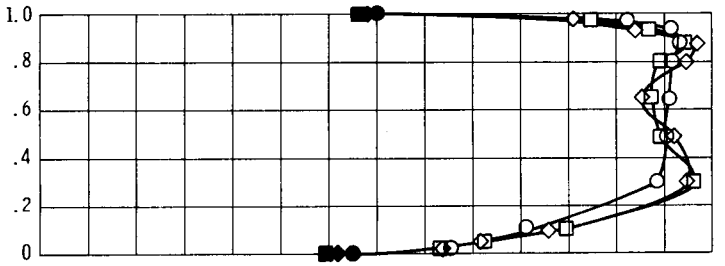

(b-2) Throat-exit rake, station 3.

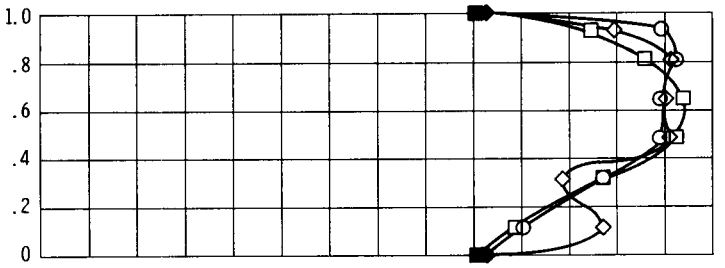

(b-3) Mid-diffuser rake, station 4.

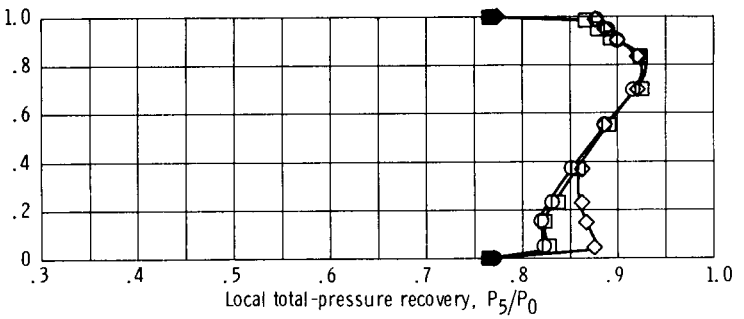

(b-4) Diffuser-exit station, rake 7, station 5.

Ratio of distance from centerbody surface to annulus height, h/H

(b) Critical inlet operating conditions.

Figure 11. - Concluded.

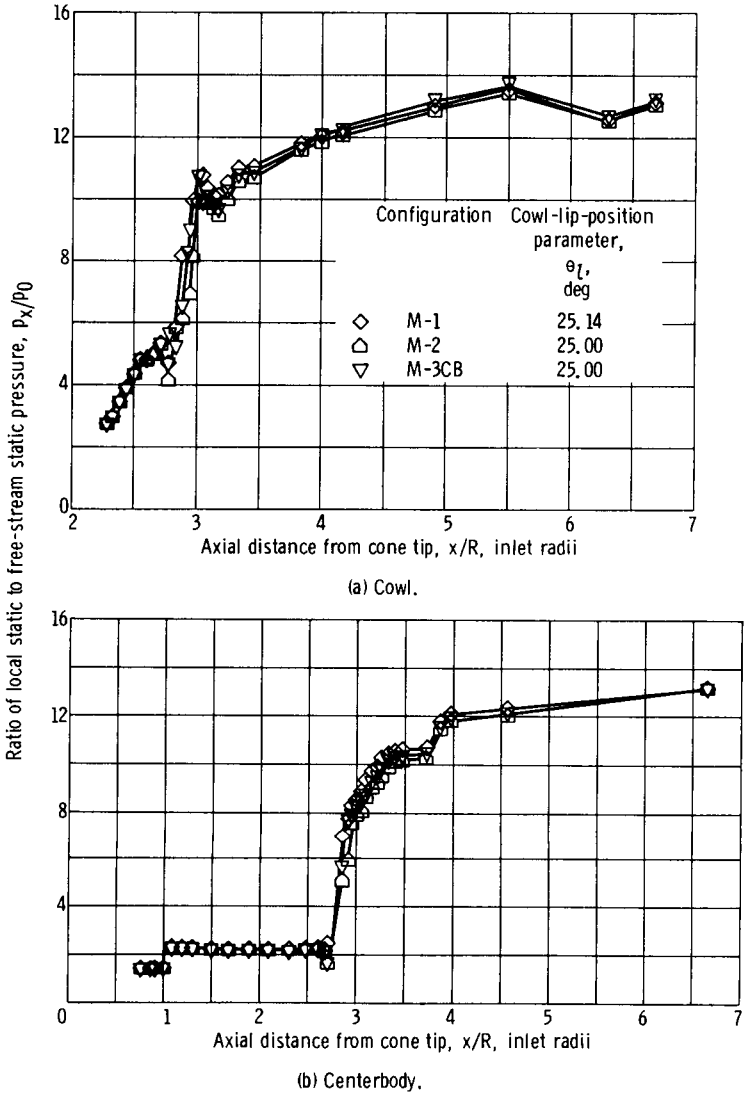

(a) Cowl.

(b) Centerbody.

Figure 12. - Diffuser static-pressure distributions for critical inlet operation. Angle of attack, 0^o.

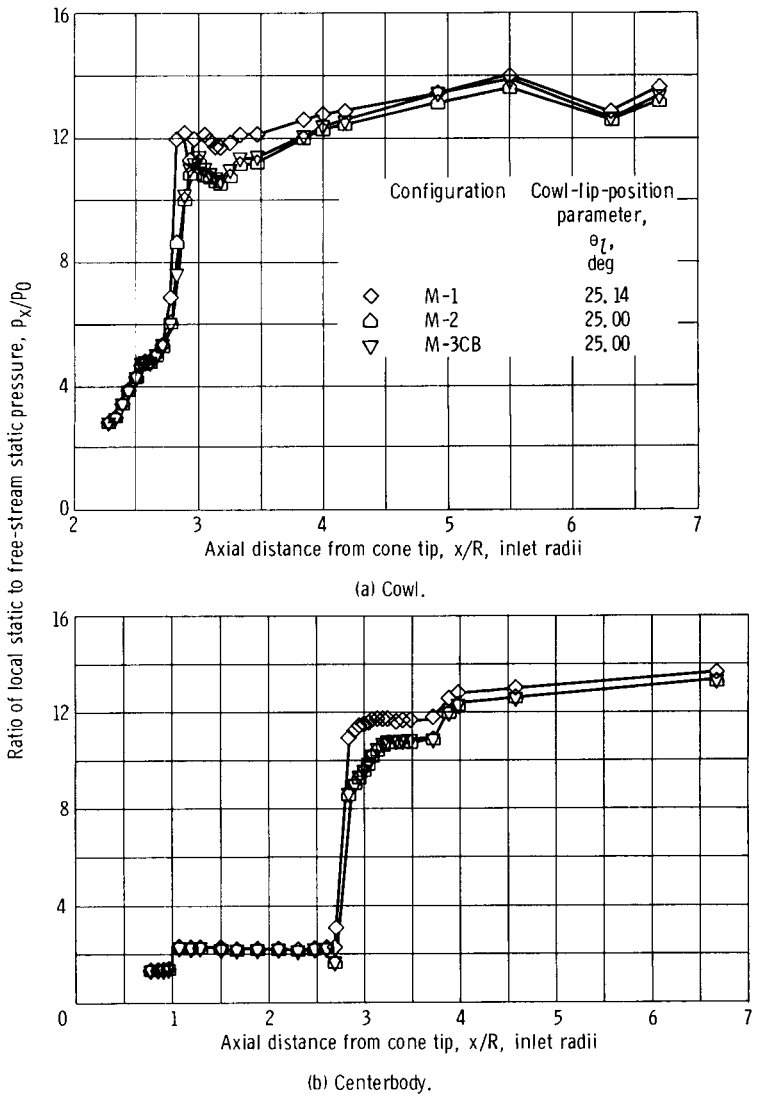

Figure 13. - Diffuser static-pressure distributions for peak inlet operation. Angle of attack, 0^0.

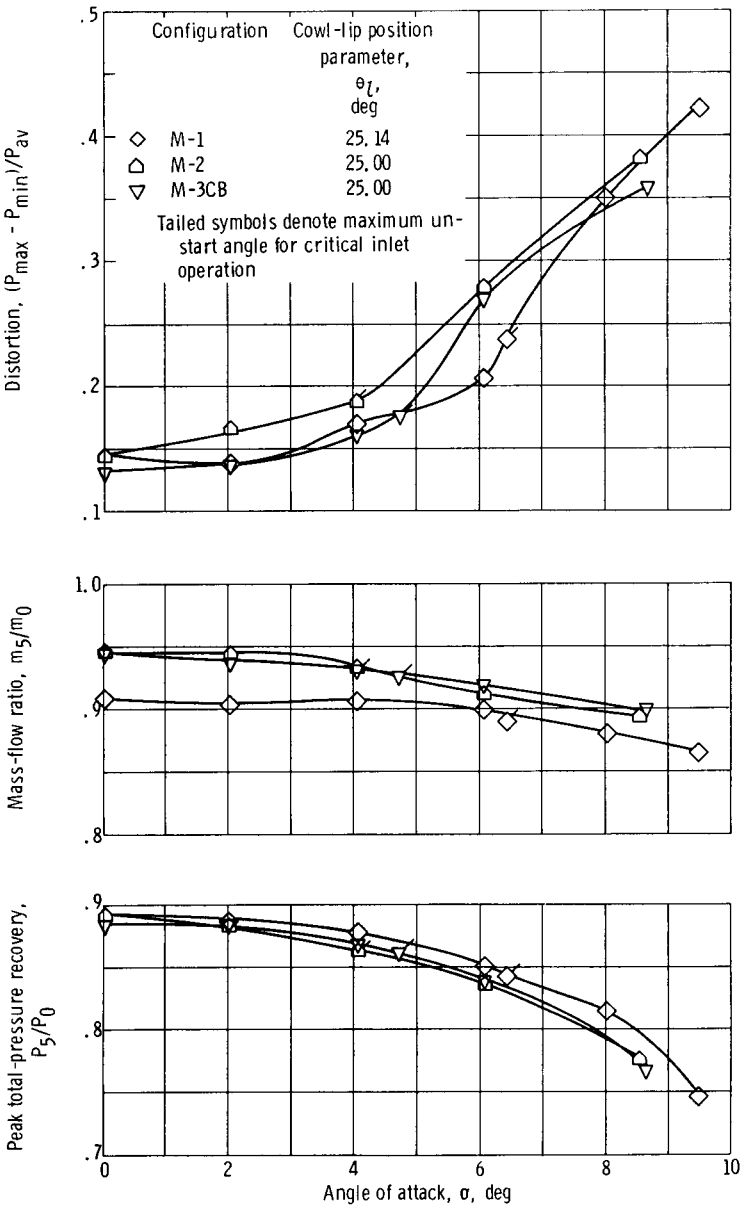

Figure 14. - Inlet performance at angle of attack.

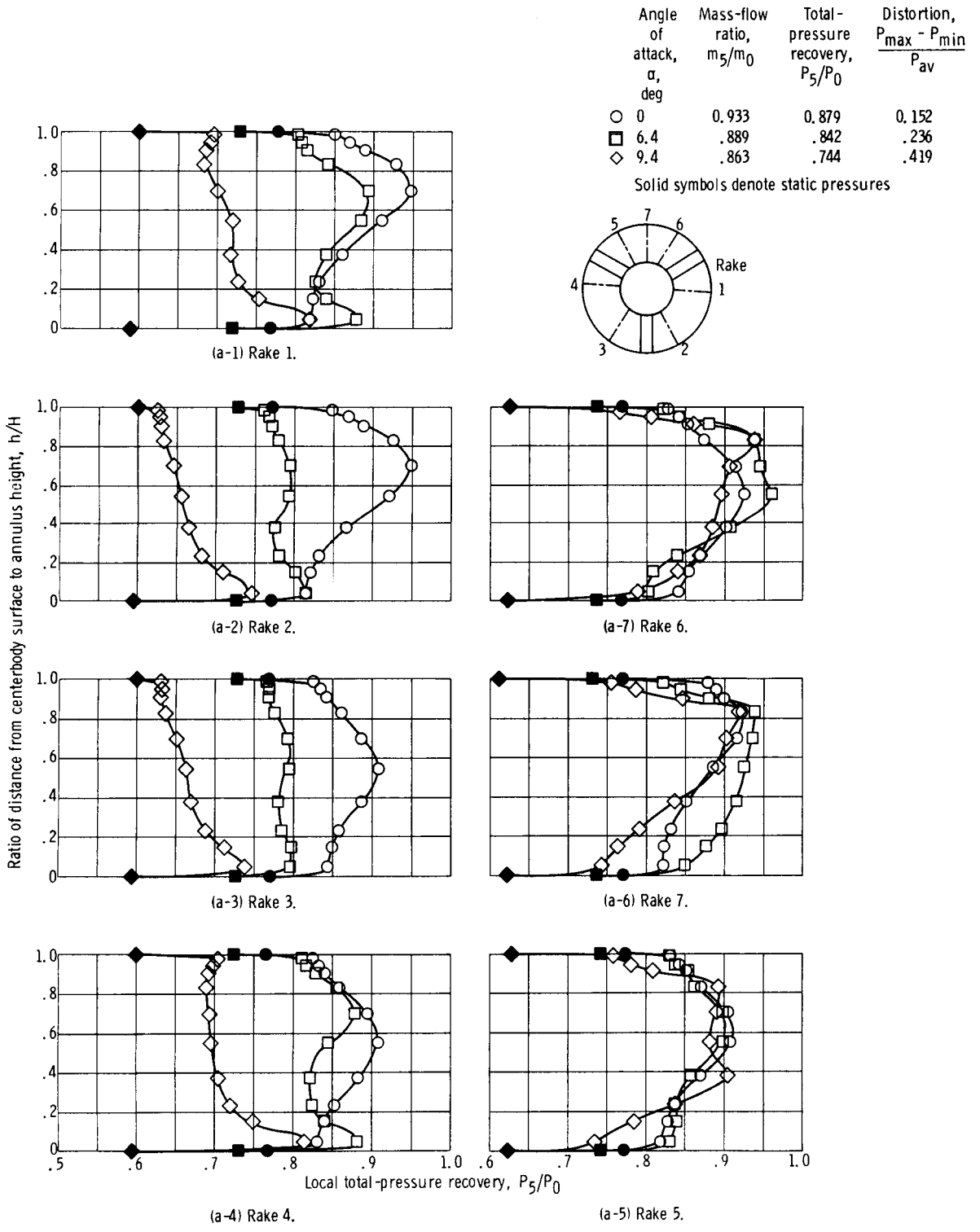

(a) Configuration M-1, $\theta_l = 25.14^0$.

Figure 15. - Effect of angle of attack on compressor-face performance, for different cowl-lip-position parameters θ_l.

	Angle of attack, α, deg	Mass-flow ratio, m_5/m_0	Total-pressure recovery, P_5/P_0	Distortion, $\frac{P_{max} - P_{min}}{P_{av}}$
○	0	0.951	0.878	0.169
□	4.0	.933	.864	.188
◇	8.5	.894	.776	.382

Solid symbols denote static pressures

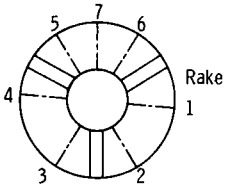

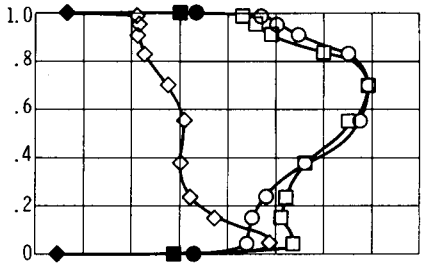

(b-1) Rake 1.

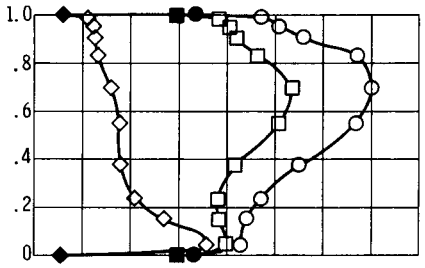

(b-2) Rake 2.

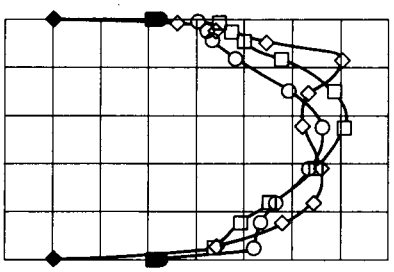

(b-7) Rake 6.

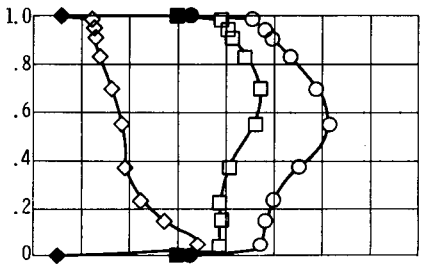

(b-3) Rake 3.

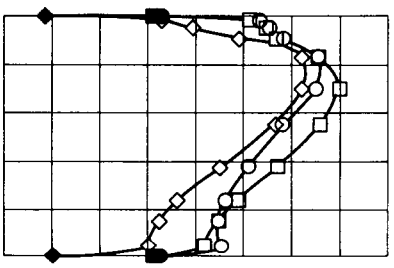

(b-6) Rake 7.

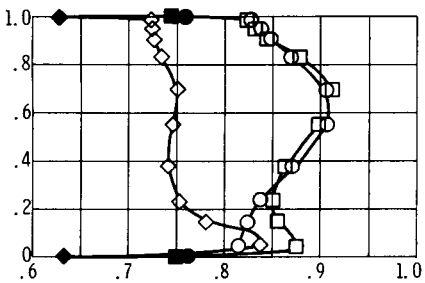

(b-4) Rake 4.

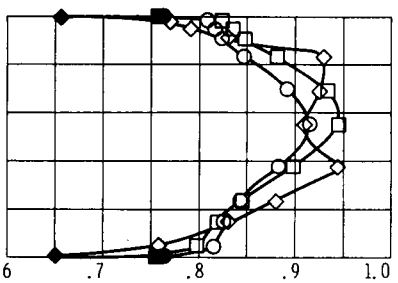

(b-5) Rake 5.

Ratio of distance from centerbody surface to annulus height, h/H

Local total-pressure recovery, P_5/P_0

(b) Configuration M-2, $\theta_l = 25.00^0$.

Figure 15. - Continued.

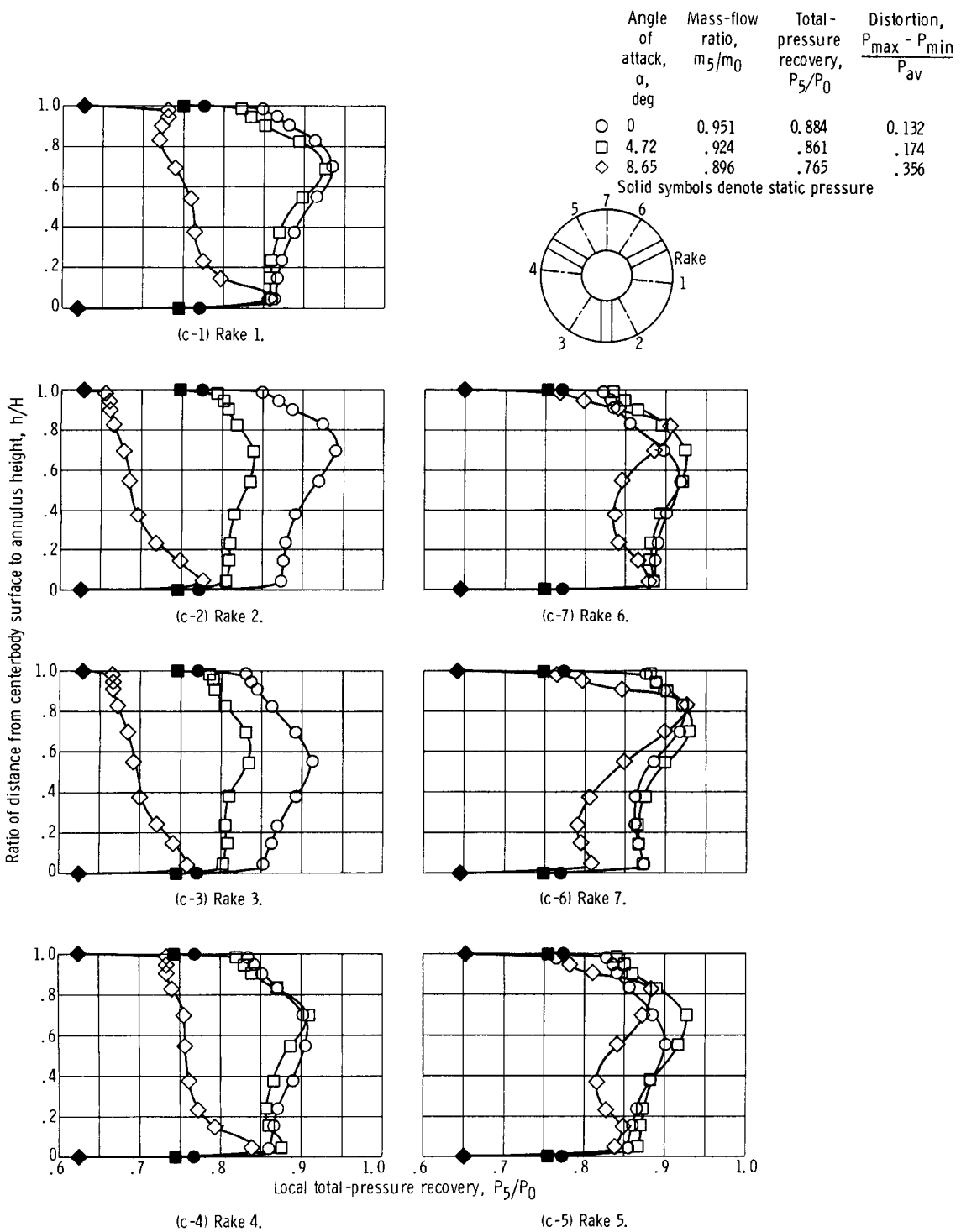

(c-1) Rake 1.

(c-2) Rake 2.

(c-7) Rake 6.

(c-3) Rake 3.

(c-6) Rake 7.

(c-4) Rake 4.

(c-5) Rake 5.

(c) Configuration M-3CB, $\theta_\ell = 25.00^0$.

Figure 15. - Concluded.

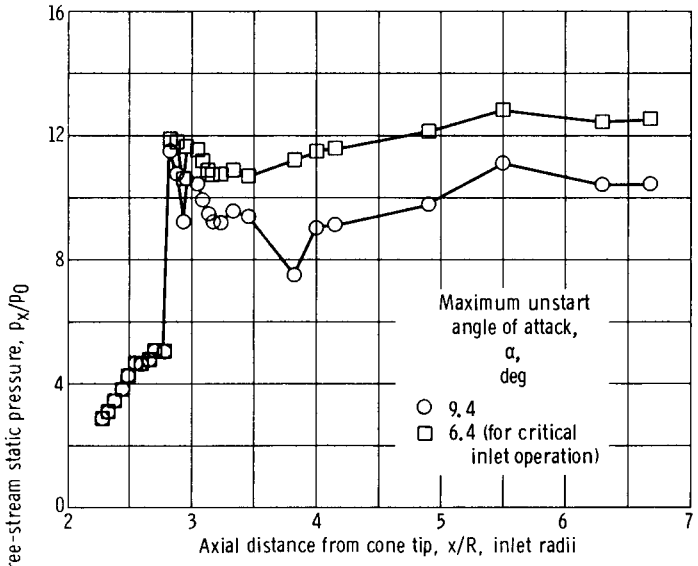

(a) Configuration M-1, cowl. Cowl-lip-position parameter, 25.14°.

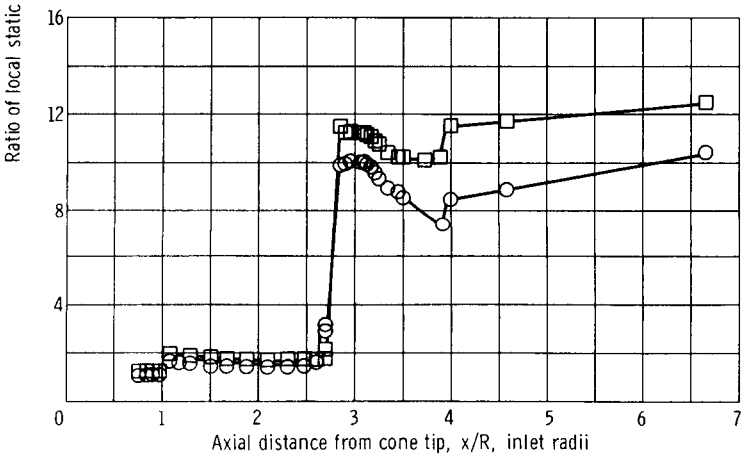

(b) Configuration M-1, centerbody. Cowl-lip-position parameter, 25.14°.

Figure 16. - Diffuser static-pressure distributions for angle-of-attack operation.

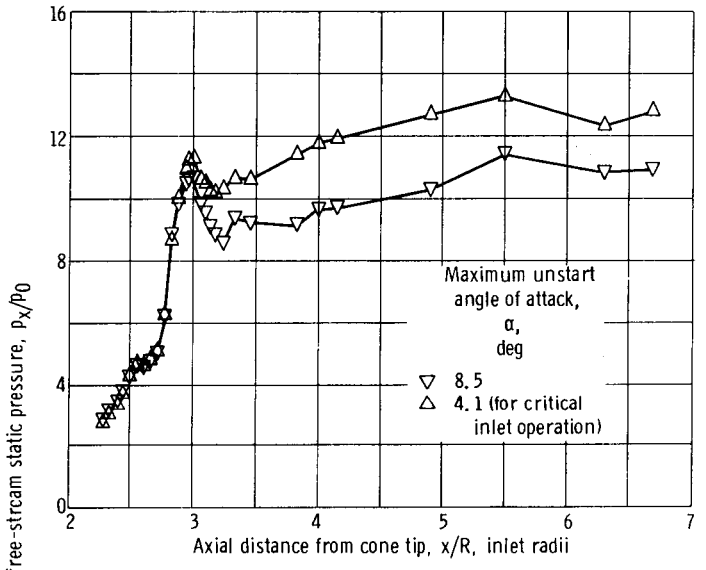

(c) Configuration M-2, cowl. Cowl-lip-position parameter, 25.00°.

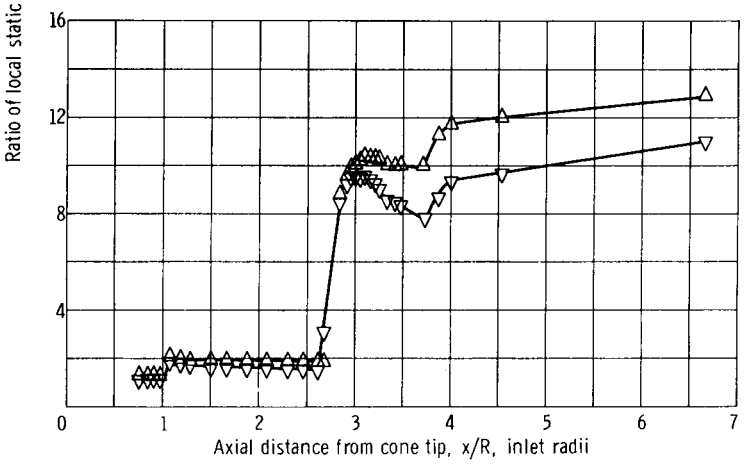

(d) Configuration M-2, centerbody. Cowl-lip-position parameter, 25.00°.

Figure 16. - Continued.

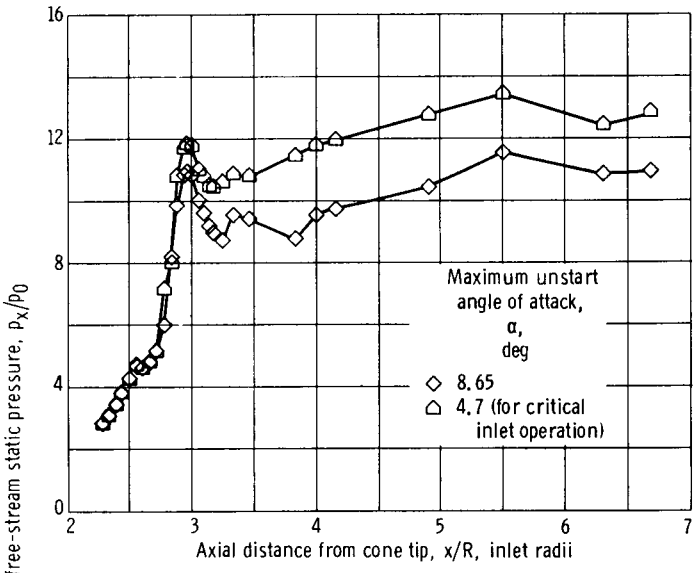

(e) Configuration M-3CB, cowl. Cowl-lip-position parameter, 25.00°.

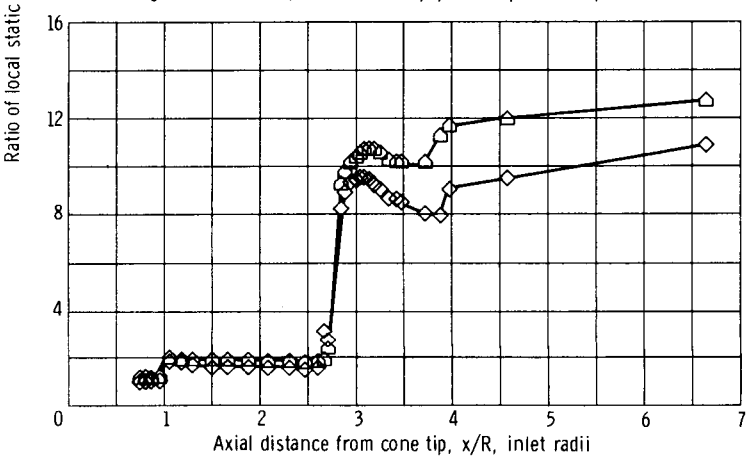

(f) Configuration M-3CB, centerbody. Cowl-lip-position parameter, 25.00°.

Figure 16. - Concluded.

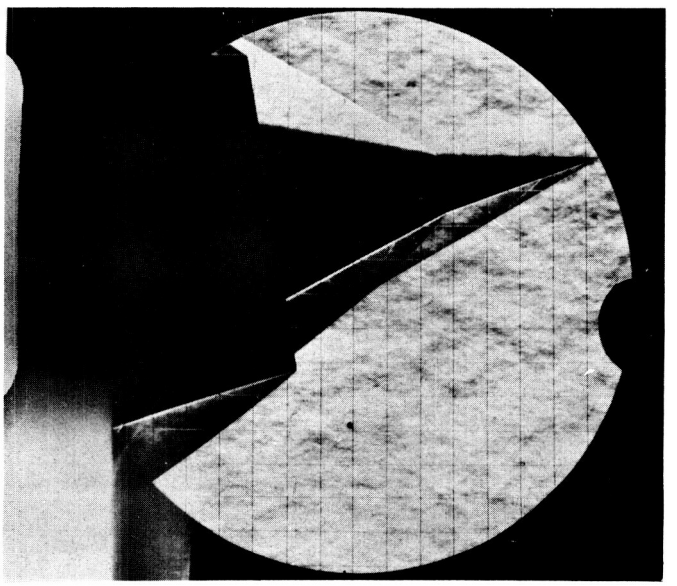

(a) Configuration M-1; $\alpha = 9.4°$; $\theta_l = 25.14°$.

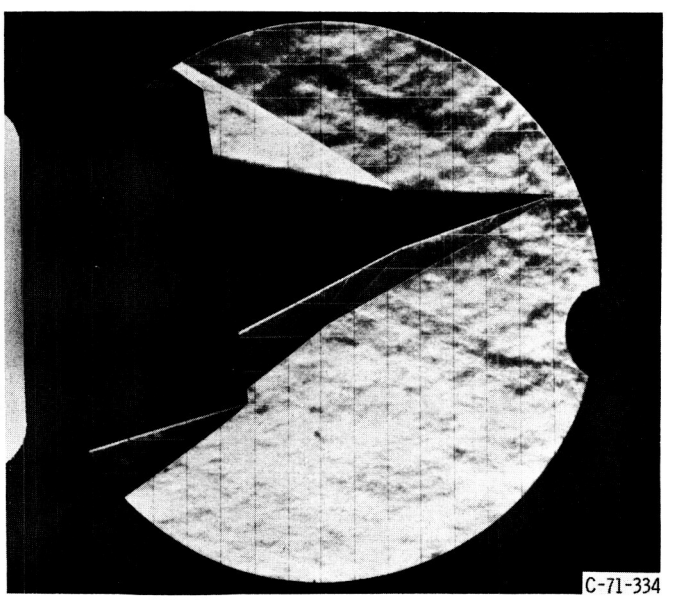

(b) Configuration M-3CB; $\alpha = 8.6°$; $\theta_l = 25.00°$.

Figure 17. - Shock patterns of focused-compresssion inlet at various angles of attack α and cowl-lip-position parameters θ_l.

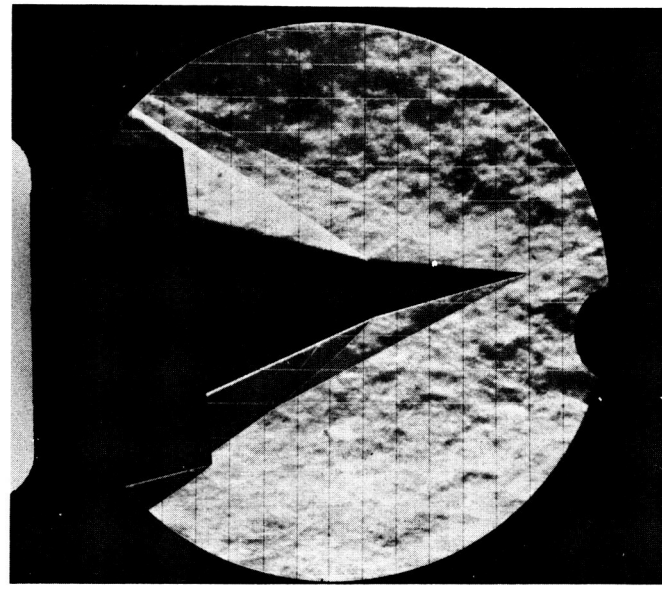

(c) Configuration M-3CB; $\alpha = 6.0°$; $\theta_l = 25.00°$.

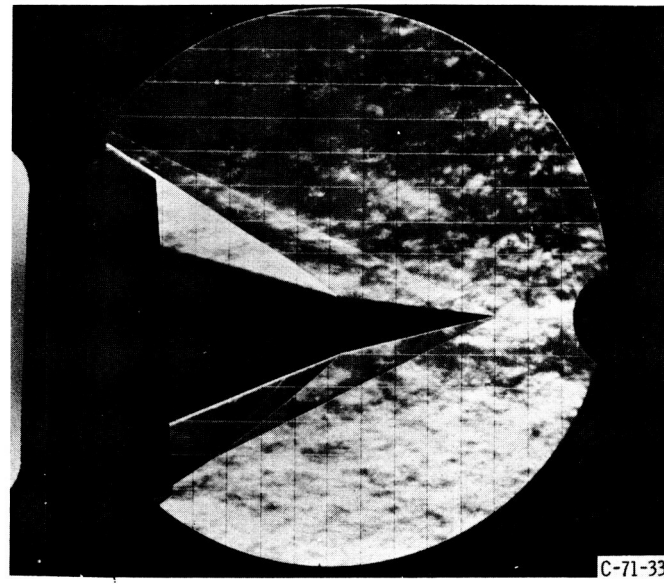

(d) Configuration M-3CB; $\alpha = 4.0°$; $\theta_l = 25.00°$.

Figure 17. - Continued.

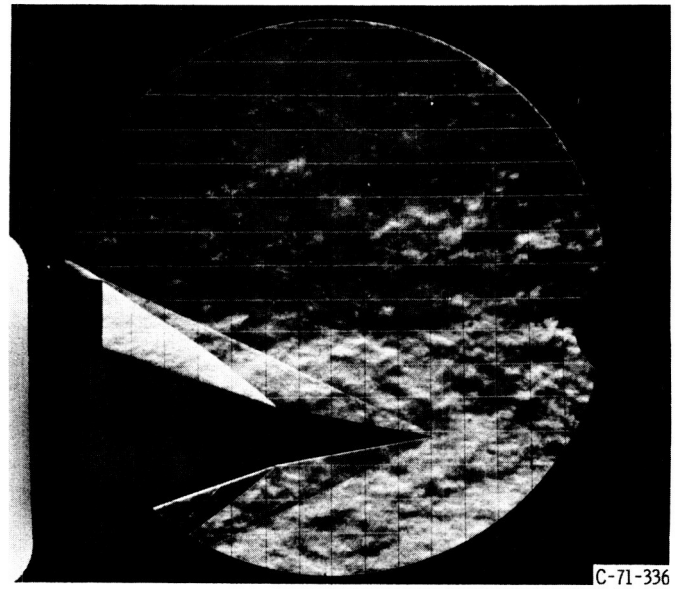

(e) Configuration M-3CB; $\alpha = 0°$; $\theta_l = 25.00°$.

Figure 17. - Concluded.

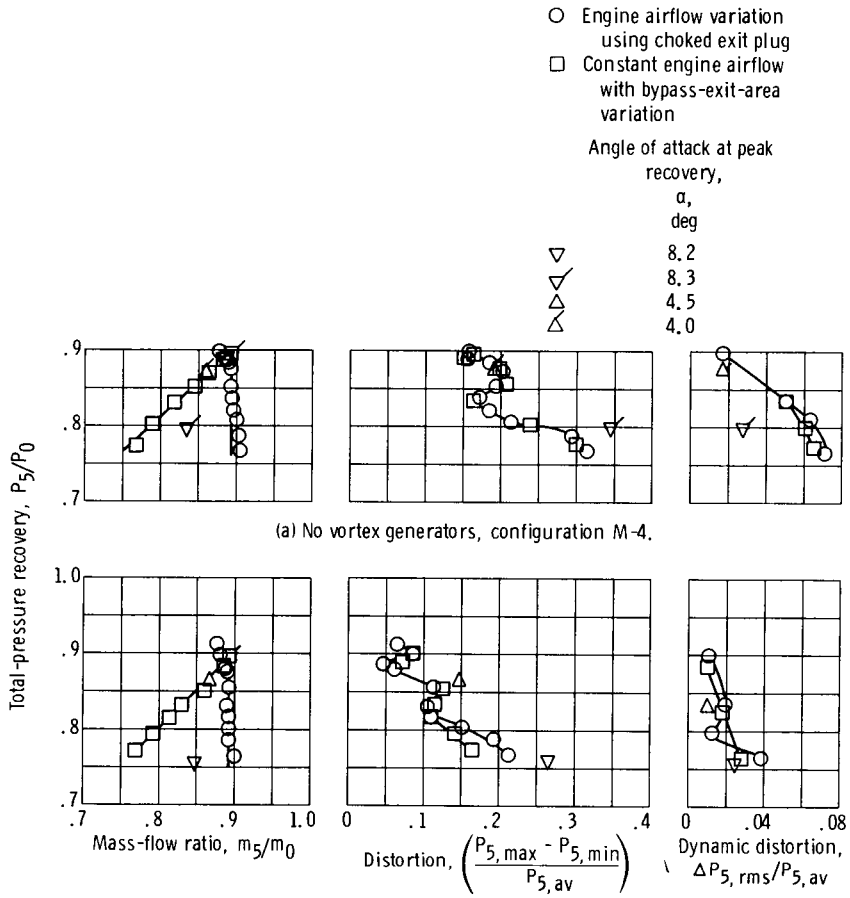

(a) No vortex generators, configuration M-4.

(b) Vortex generators on cowl and centerbody, configuration M-4CCB.

Figure 18. - Overall performance of inlet configurations M-4 and M-4CCB. Cowl-lip-position parameter, 25.00^0; ejector area to capture area, 0.0103; engine-corrected airflow, 35.5 pounds per second (16.1 kg/sec).

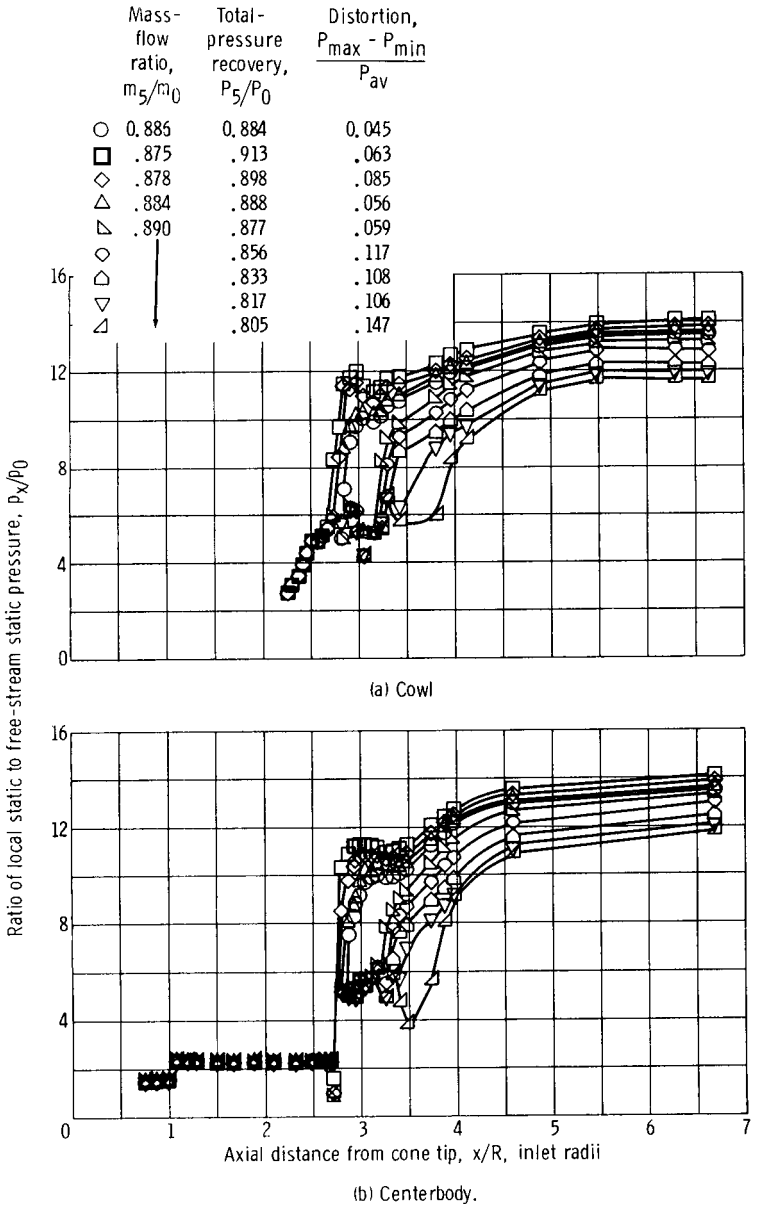

Figure 19. - Diffuser static-pressure distributions for various engine-corrected airflows. Configuration M-4CCB; angle of attack 0^0; cowl-lip-position parameter, 25.00^0.

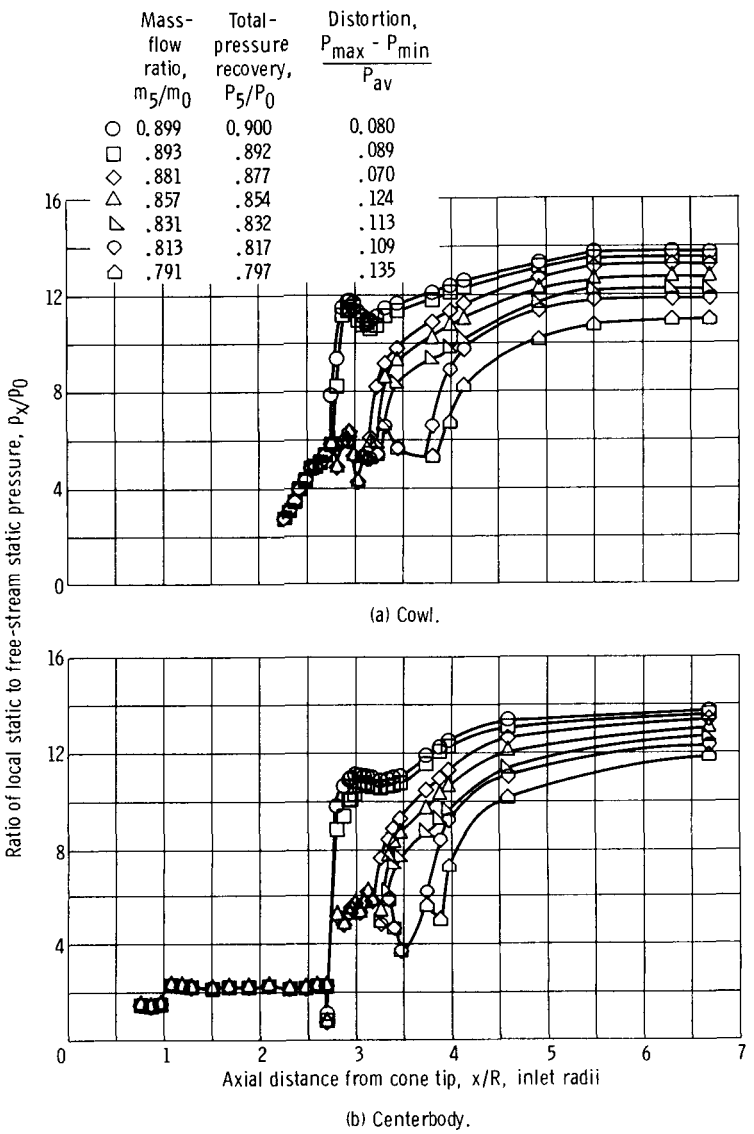

Figure 20. - Diffuser static-pressure distributions for various bypass door settings. Configuration M-4CCB; angle of attack, 0^0; cowl-lip-position parameter, 25.00^0.

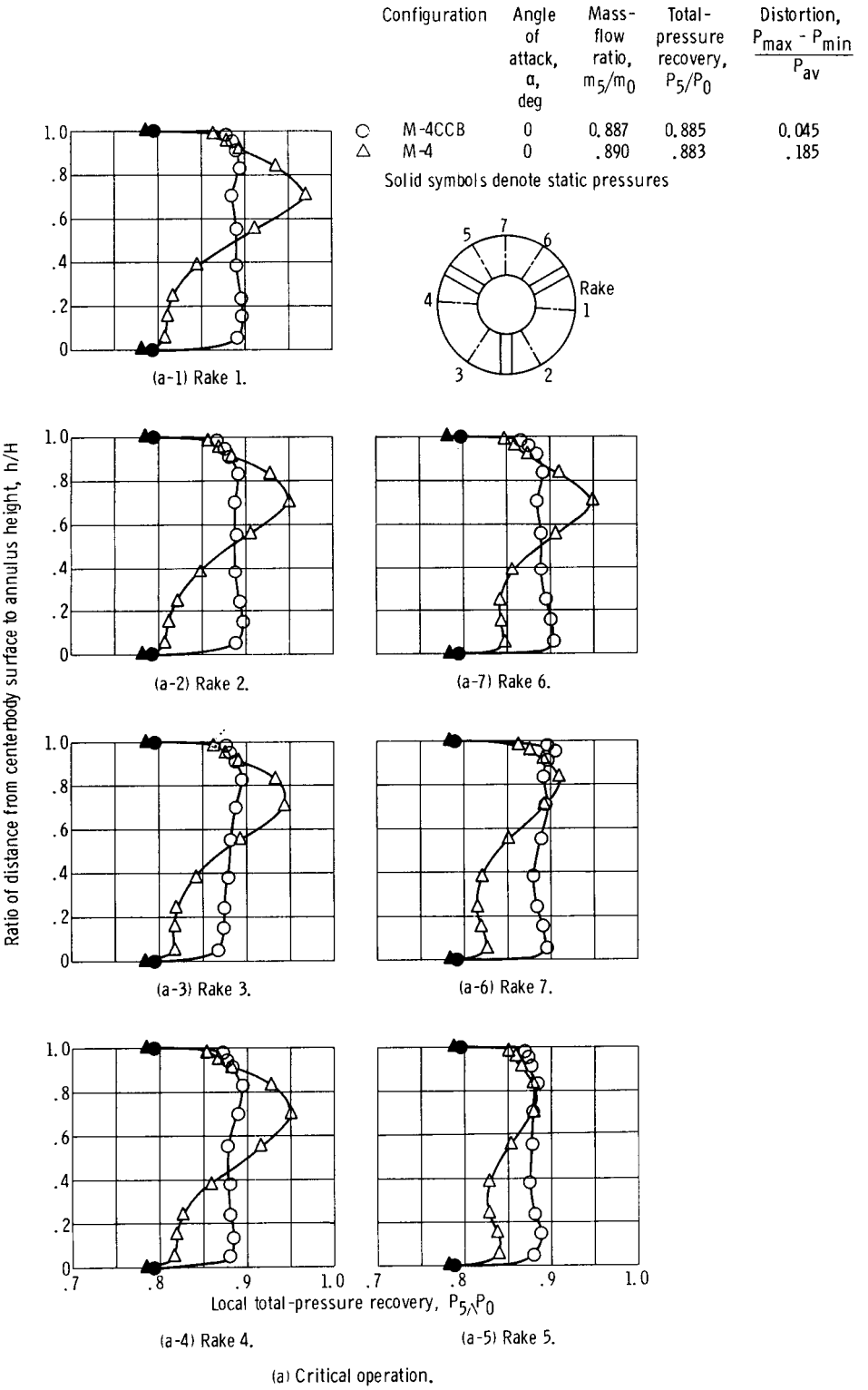

(a) Critical operation.

Figure 21. - Effect of vortex generators on angle-of-attack performance. Cowl-lip-parameter, 25.00°.

Configuration	Angle of attack, α, deg	Mass-flow ratio, m_5/m_0	Total-pressure recovery, P_5/P_0	Distortion, $\frac{P_{max} - P_{min}}{P_{av}}$
○ M-4CCB	4.57	0.865	0.863	0.146
△ M-4	4.04	.860	.875	.187

Solid symbols denote static pressures

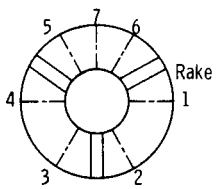

(b-1) Rake 1.

(b-2) Rake 2.

(b-7) Rake 6.

(b-3) Rake 3.

(b-6) Rake 7.

(b-4) Rake 4.

(b-5) Rake 5.

(b) Maximum angle of attack for critical inlet operation.

Figure 21. - Continued.

Configuration		Angle of attack, α, deg	Mass-flow ratio, m_5/m_0	Total-pressure recovery, P_5/P_0	Distortion, $\frac{P_{max} - P_{min}}{P_{av}}$
○	M-4CCB	8.17	0.846	0.758	0.262
△	M-4	8.32	.833	.796	.343

Solid symbols denote static pressures

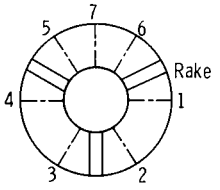

(c-1) Rake 1.

(c-2) Rake 2.

(c-3) Rake 3.

(c-4) Rake 4.

(c-5) Rake 5.

(c-6) Rake 7.

(c-7) Rake 6.

(c) Maximum angle of attack.

Figure 21. - Concluded.

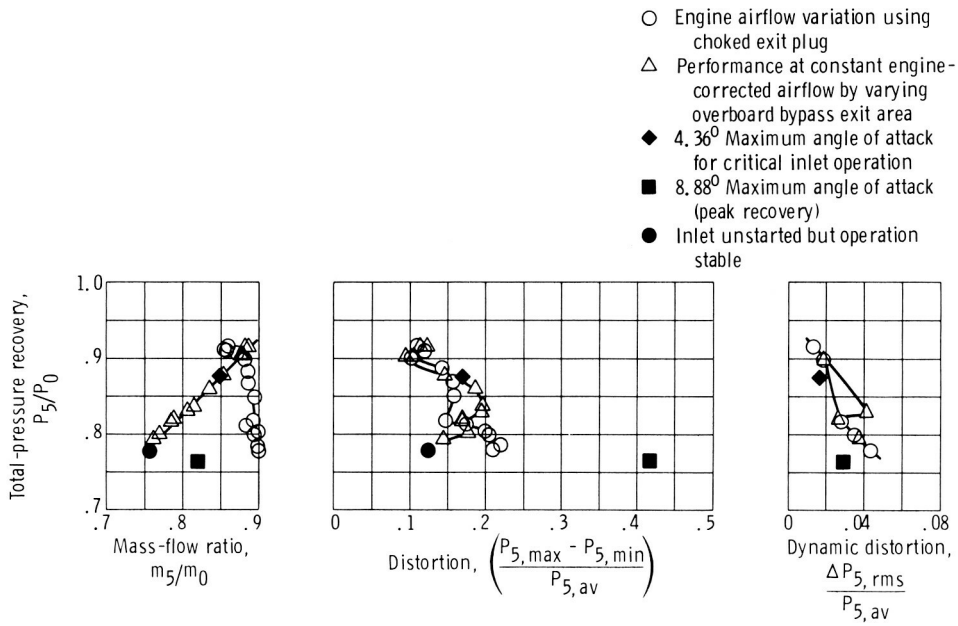

Figure 22. - Overall performance of inlet configuration M-3CB with bypass flow. Cowl-lip-position parameter, 25.00°; ejector area to capture area, 0.0103; engine-corrected airflow, 34.5 pounds per second (15.65 kg/sec).

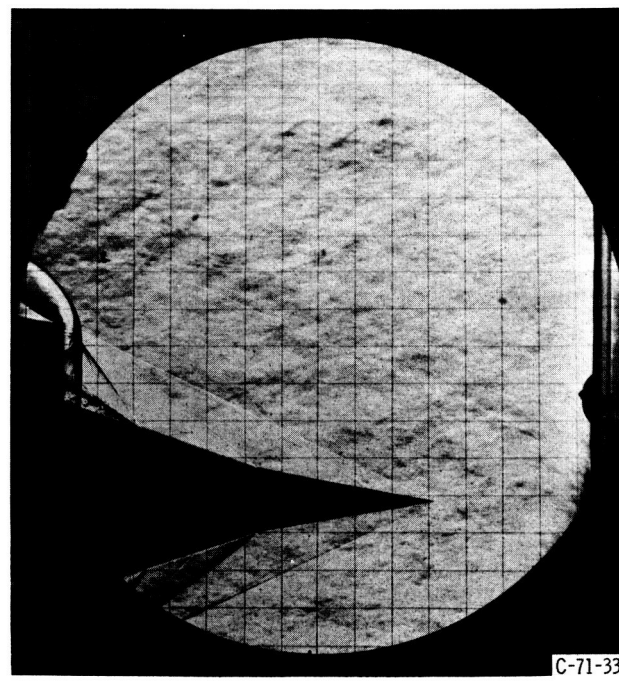

Figure 23. - Inlet unstarted but stable operation. Configuration M-3CB; angle of attack, 0°; cowl-lip-position parameter, 25.00°.

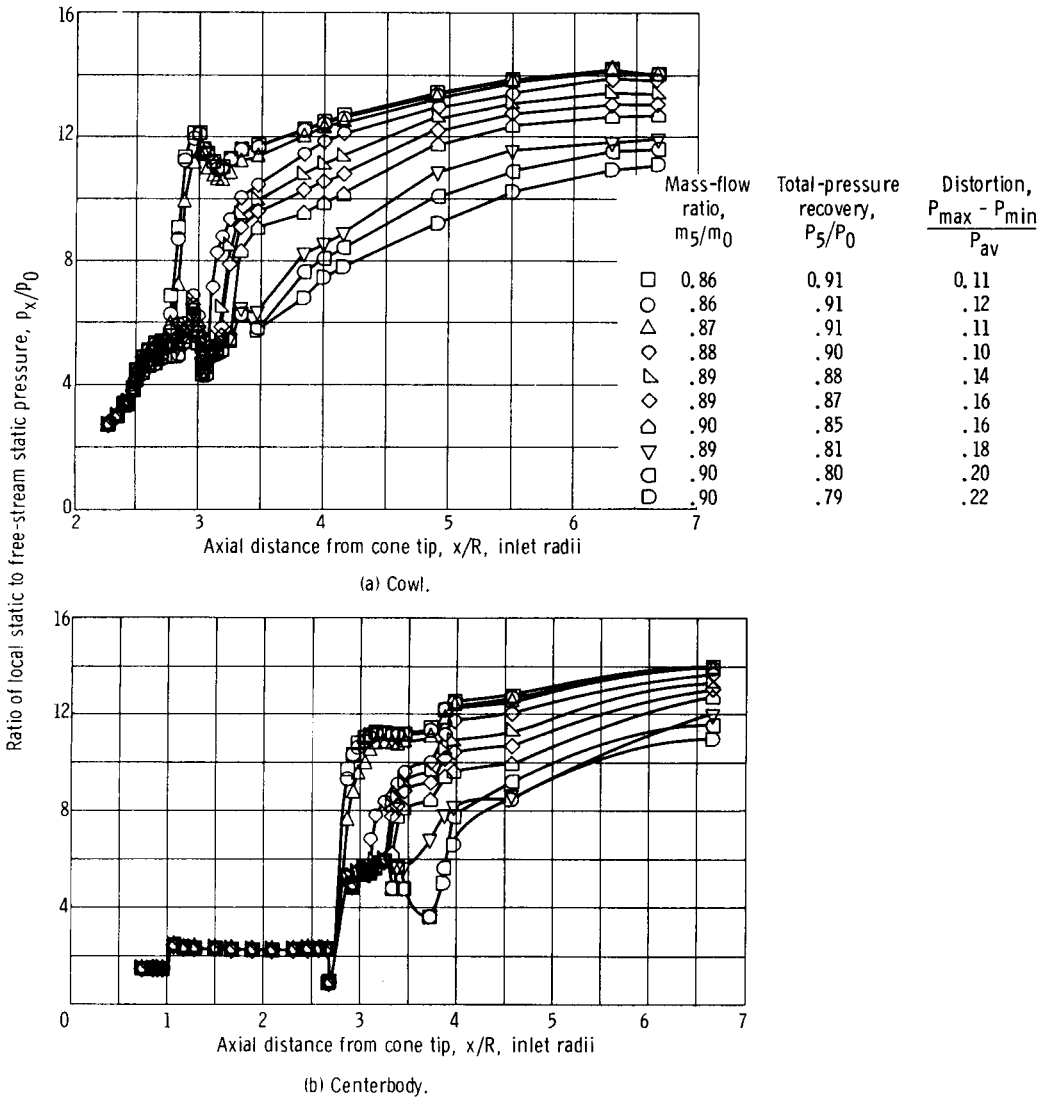

Figure 24. - Diffuser static-pressure distributions for various engine-corrected airflows. Configuration M-3CB; angle of attack, 0^0; cowl-lip-position parameter, 25.00^0.

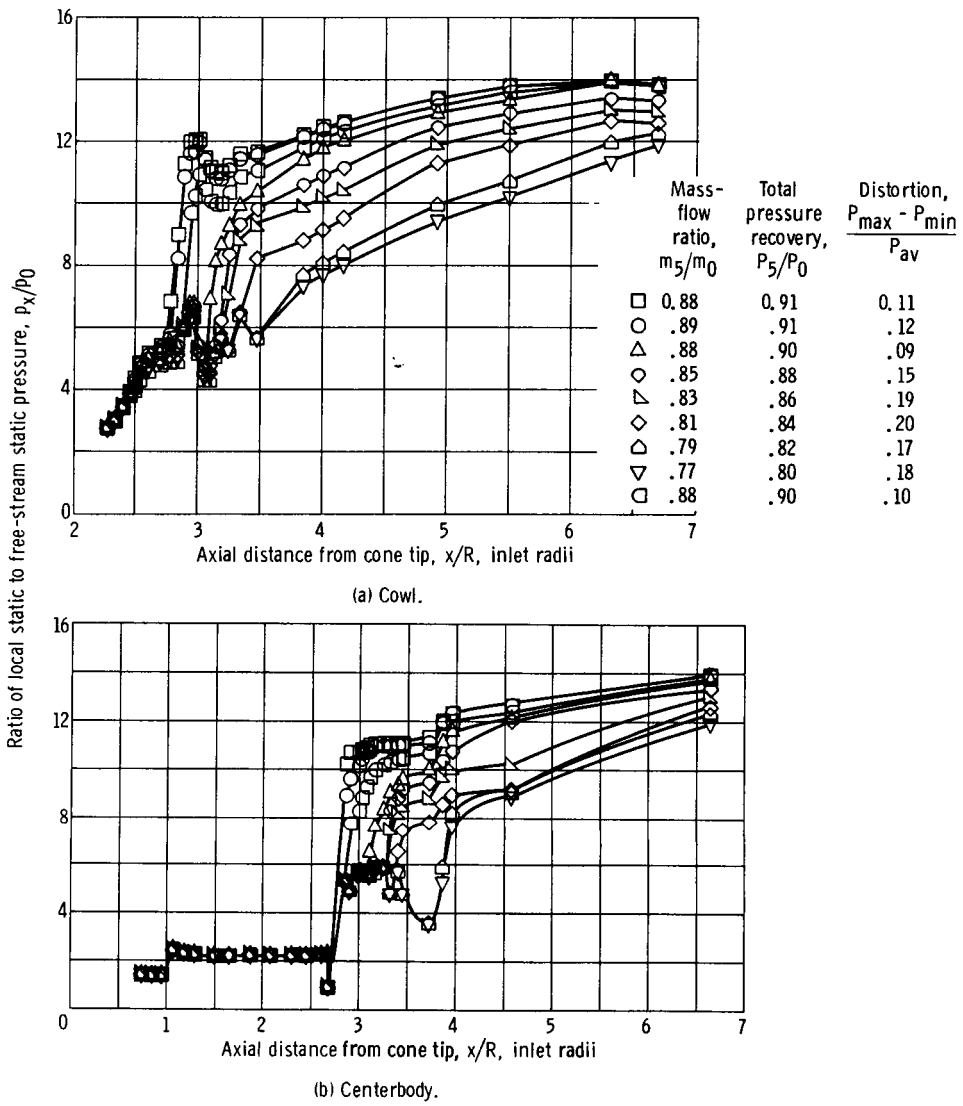

(a) Cowl.

(b) Centerbody.

Figure 25. - Diffuser static-pressure distributions for various bypass door settings. Configuration M-3CB; angle of attack, 0^0; cowl-lip-position parameter, 25.00^0.

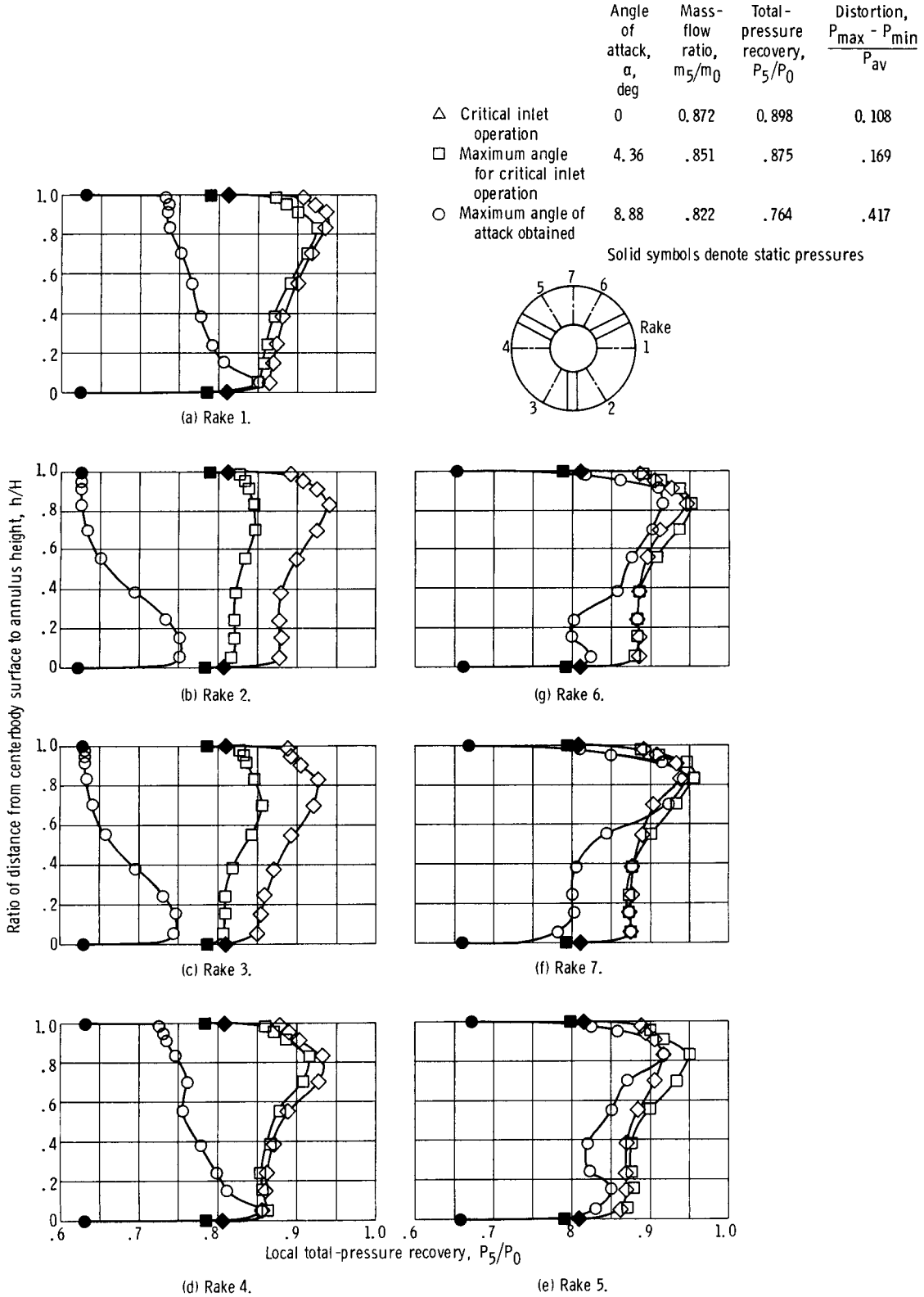

Figure 26. - Effect of angle of attack on compressor-face performance with bypass flow. Configuration M-3CB; cowl-lip-position parameter, 25.00°.

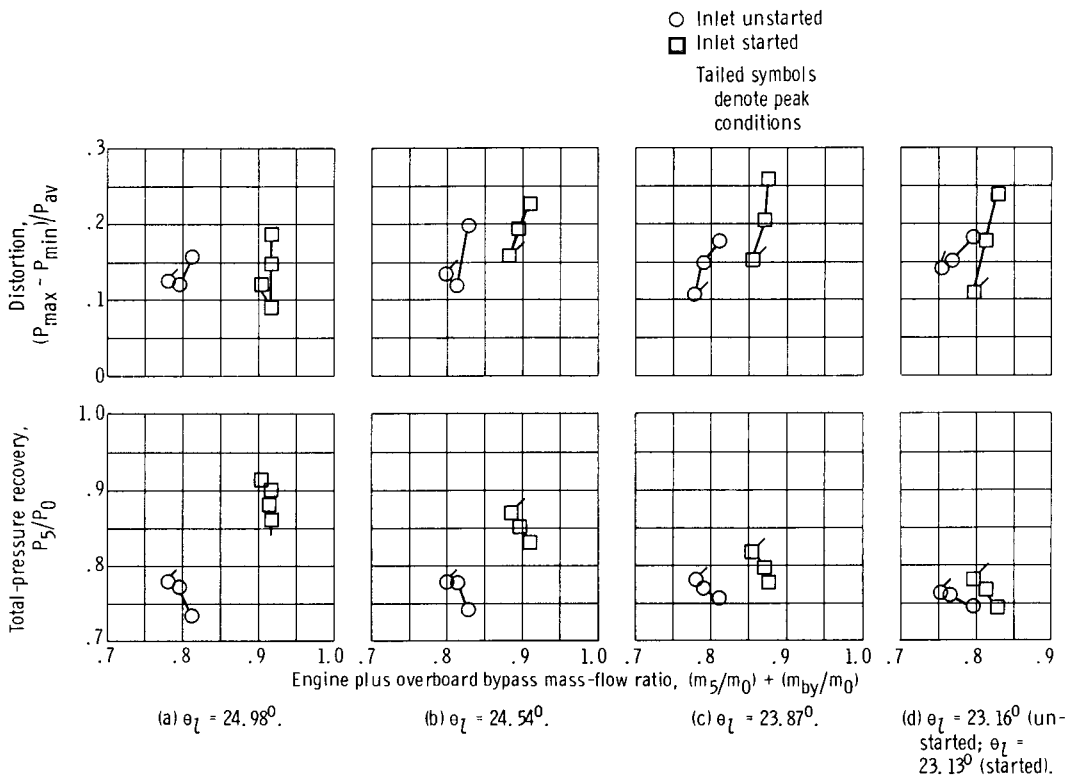

Figure 27. - Inlet performance during restart cycle at Mach 2.50. Inlet configuration M-3CB; angle of attack, 0^0; various values of cowl-lip-position parameter θ_l.

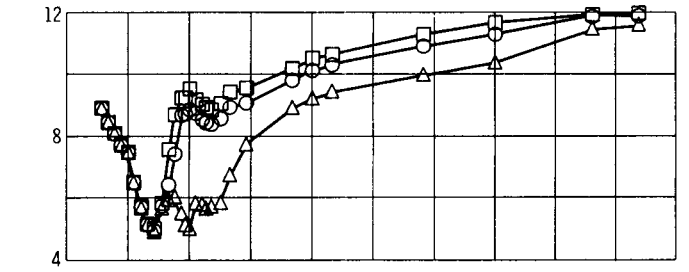

	Total-pressure recovery, P_5/P_0	Engine plus overboard bypass mass-flow ratio, $(m_5/m_0)/(m_{by}/m_0)$
□	0.78	0.781
○	.77	.794
△	.75	.811

(a) Cowl-lip-position parameter, 24.98°; unstarted.

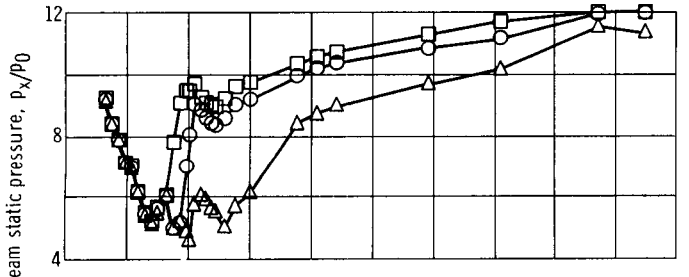

□	0.78	0.799
○	.78	.814
△	.74	.827

(b) Cowl-lip-position parameter, 24.54°; unstarted.

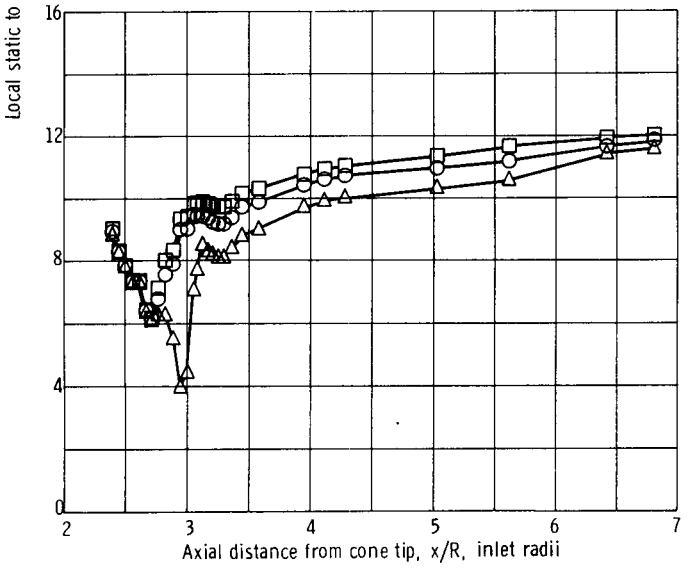

□	0.78	0.780
○	.77	.788
△	.76	.809

(c) Cowl-lip-position parameter, 23.87°; unstarted.

Figure 28. - Internal cowl-surface, static-pressure distributions during inlet restart sequence. Configuration M-3CB.

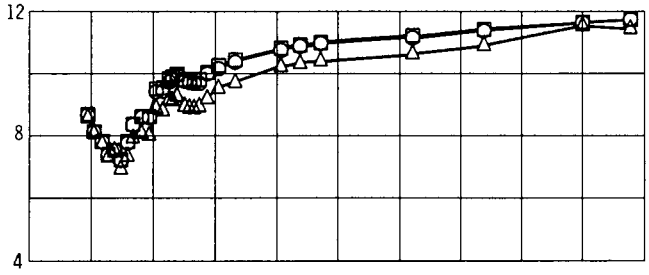

Total-pressure recovery, P_5/P_0	Engine plus overboard bypass mass-flow ratio, $(m_5/m_0)/(m_{by}/m_0)$
□ 0.76	0.753
○ .76	.766
△ .75	.794

(d) Cowl-lip-position parameter, 23.16°; unstarted.

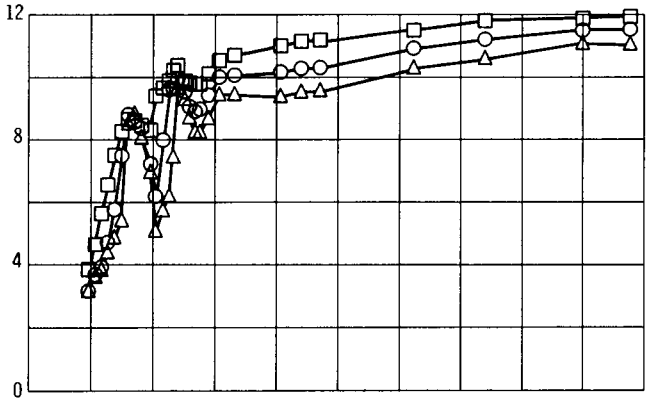

□ 0.78	0.795
○ .77	.812
△ .75	.827

(e) Cowl-lip-position parameter, 23.13; started.

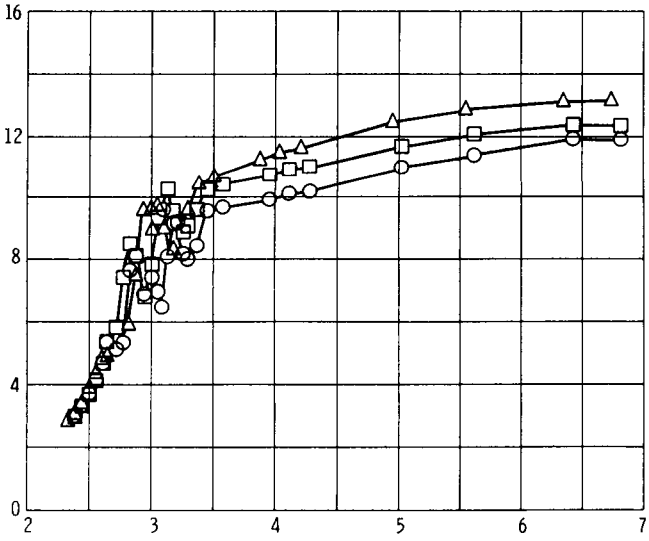

□ 0.82	0.853
○ .80	.868
△ .87	.874

Ratio of local static to free-stream static pressure, p_x/p_0

(f) Cowl-lip-position parameter, 23.87°; started.

Figure 28. - Continued.

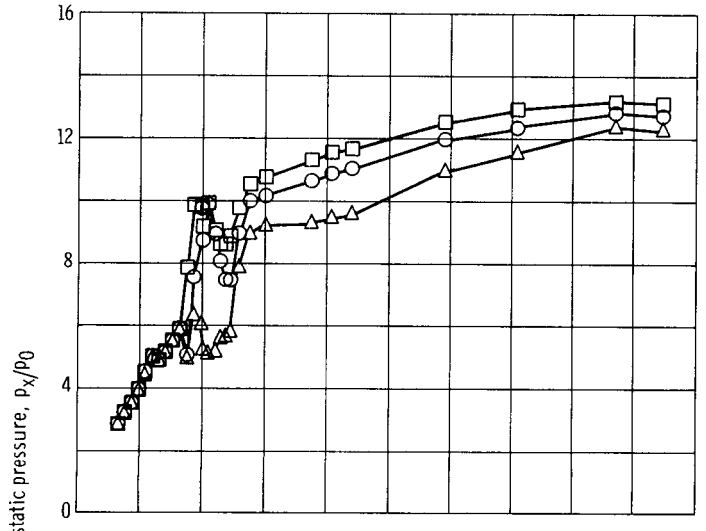

Total-pressure recovery, P_5/P_0	Engine plus overboard bypass mass-flow ratio, $(m_5/m_0)/(m_{by}/m_0)$
□ 0.87	0.884
○ .85	.894
△ .82	.910

(g) Cowl-lip-position parameter, 24.54°; started.

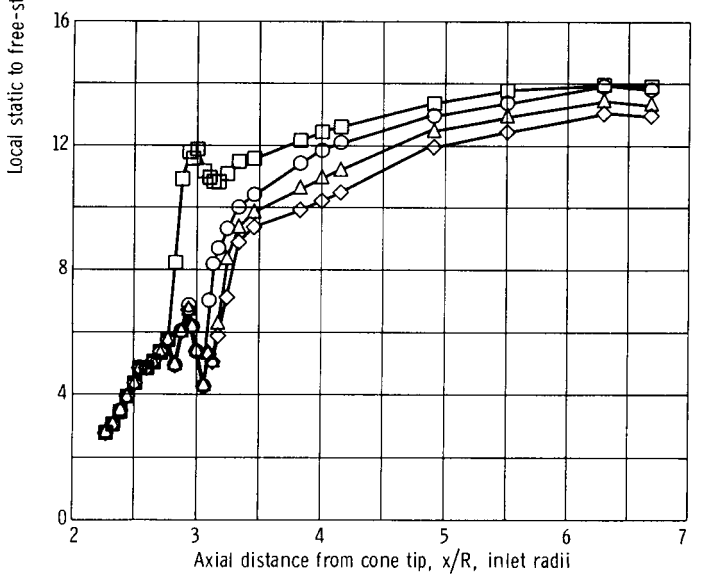

□ 0.91	.903
○ .90	.916
△ .88	.914
◇ .86	.916

(h) Cowl-lip-position parameter, 24.98°; started.

Figure 28. - Concluded.

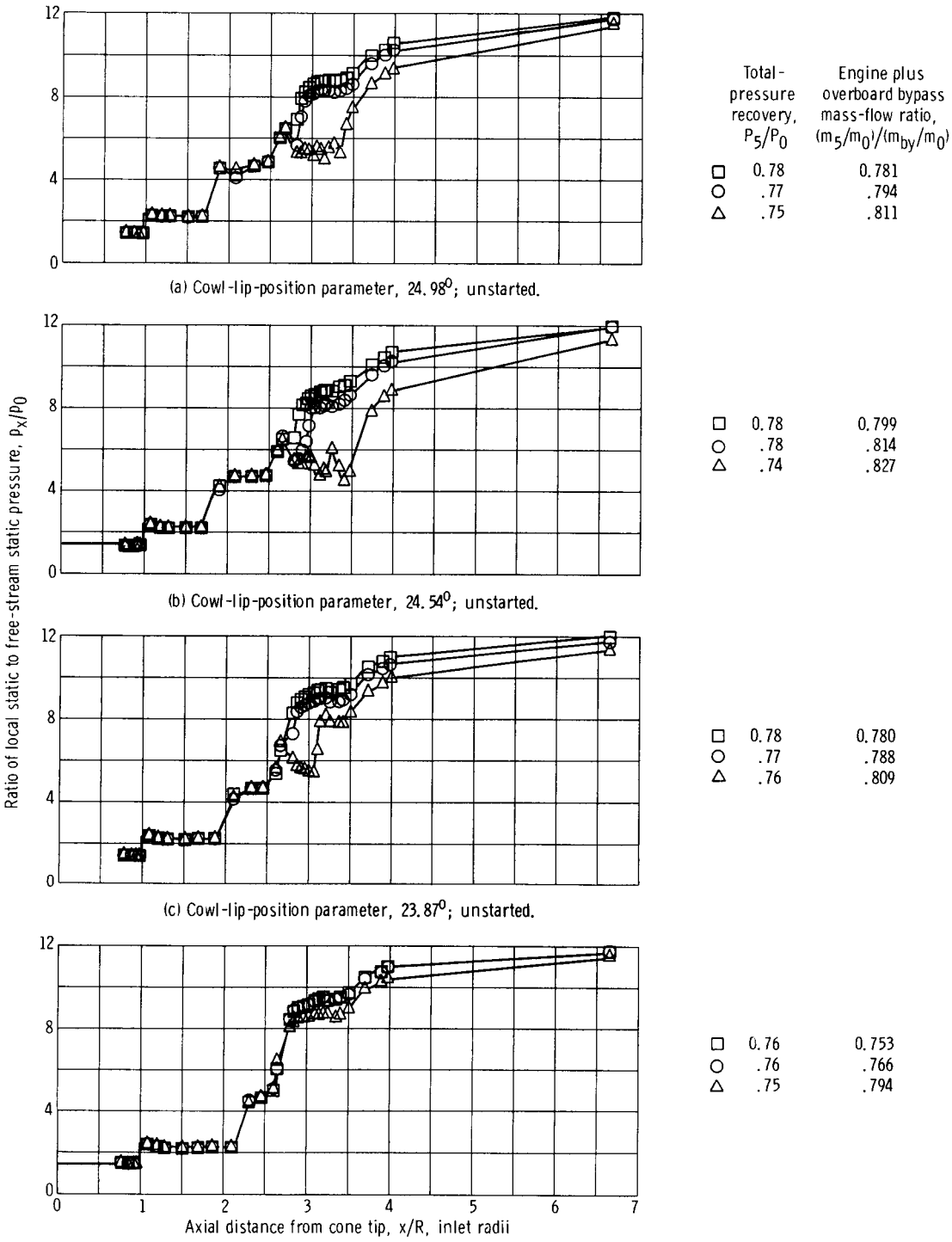

(a) Cowl-lip-position parameter, 24.98°; unstarted.

(b) Cowl-lip-position parameter, 24.54°; unstarted.

(c) Cowl-lip-position parameter, 23.87°; unstarted.

(d) Cowl-lip-position parameter, 23.16°; unstarted.

Figure 29. - Centerbody surface static-pressure distributions during inlet restart sequence. Configuration M-3CB.

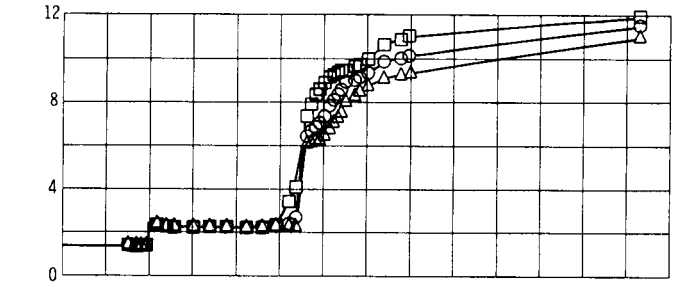

Total-pressure recovery, P_5/P_0	Engine plus overboard bypass mass-flow ratio, $(m_5/m_0)/(m_{by}/m_0)$
□ 0.78	0.795
○ .77	.812
△ .75	.827

(e) Cowl-lip-position parameter, 23.13°; started.

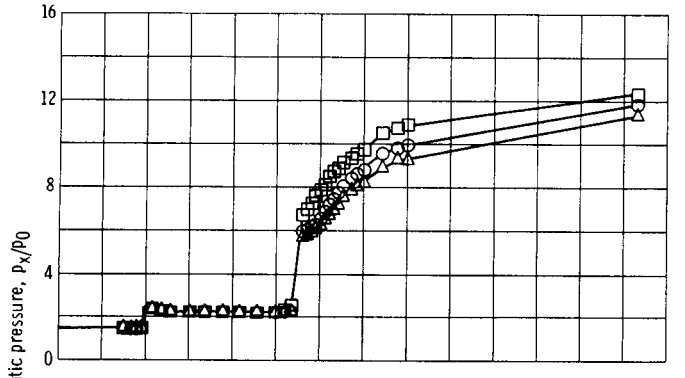

□ 0.82	0.853
○ .80	.868
△ .87	.874

(f) Cowl-lip-position parameter, 23.87°; started.

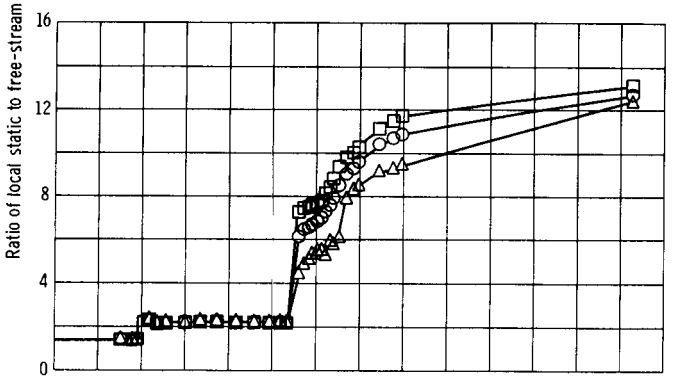

□ 0.87	0.884
○ .85	.894
△ .82	.910

(g) Cowl-lip-position parameter, 24.54°; started.

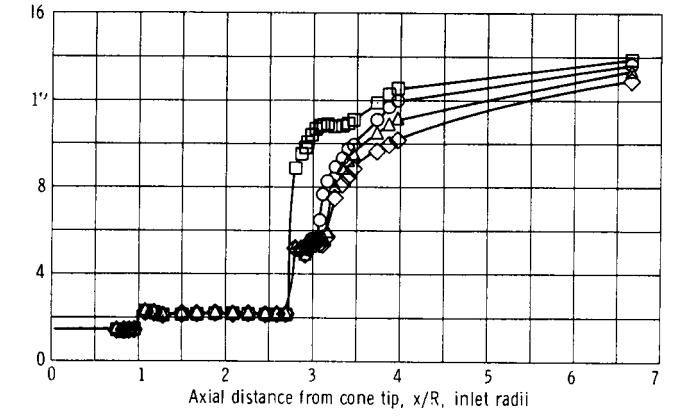

□ 0.91	0.903
○ .90	.916
△ .88	.914
◇ .86	.916

(h) Cowl-lip-position parameter, 24.98°; started.

Figure 29. - Concluded.

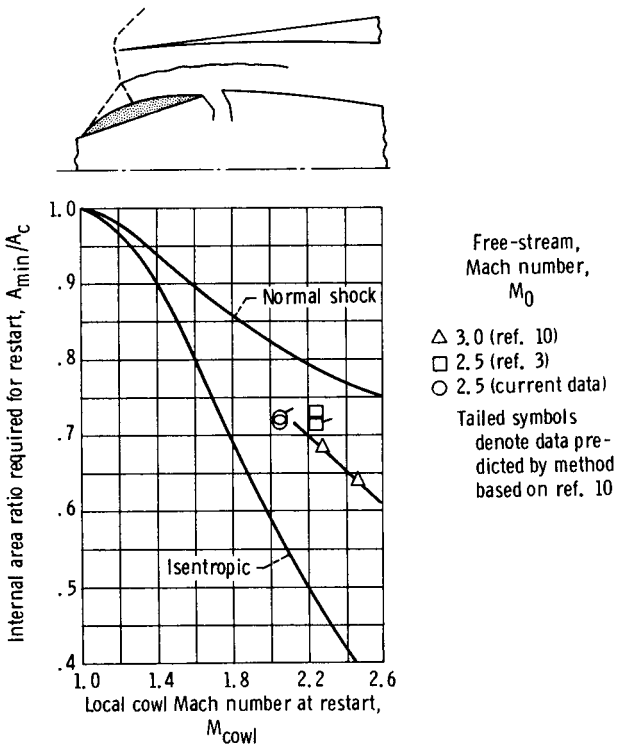

Figure 30. - Comparison of actual to predicted restart area ratio.